Journal of Medicinal Chemistry

Article

pubs.acs.org/jmc

Discovery of Selective Small-Molecule Inhibitors for the β-Catenin/T-Cell Factor Protein−Protein Interaction through the Optimization of the Acyl Hydrazone Moiety

J. Leon Catrow,[†] Yongqiang Zhang,[†] Min Zhang, and Haitao Ji*

Department of Chemistry, Center for Cell and Genome Science, University of Utah, 315 South 1400 East, Salt Lake City, Utah 84112−0850, United States

Supporting Information

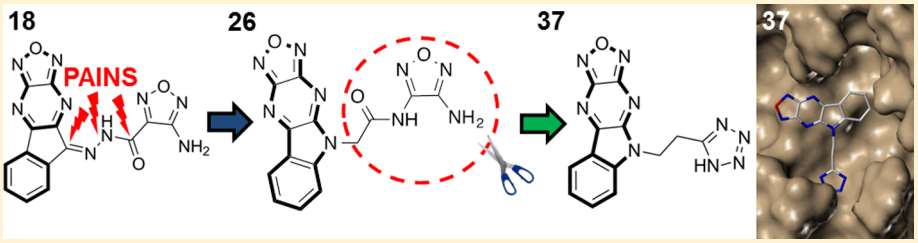

ABSTRACT: Acyl hydrazone is an important functional group for the discovery of bioactive small molecules. This functional group is also recognized as a pan assay interference structure. In this study, a new small-molecule inhibitor for the β-catenin/Tcf protein−protein interaction (PPI), ZINC02092166, was identified through AlphaScreen and FP assays. This compound contains an acyl hydrazone group and exhibits higher inhibitory activities in cell-based assays than biochemical assays. Inhibitor optimization resulted in chemically stable derivatives that disrupt the β-catenin/Tcf PPI. The binding mode of new inhibitors was characterized by site-directed mutagenesis and structure−activity relationship studies. This series of inhibitors with a new scaffold exhibits dual selectivity for β-catenin/Tcf over β-catenin/cadherin and β-catenin/APC PPIs. One derivative of this series suppresses canonical Wnt signaling, downregulates the expression of Wnt target genes, and inhibits the growth of cancer cells. This compound represents a solid starting point for the development of potent and selective β-catenin/Tcf inhibitors.

INTRODUCTION

The formation of an acyl hydrazone moiety has emerged as an important strategy in dynamic combinatorial chemistry (DCC) to discover bioactive small molecules for protein targets.[1−3] The acyl hydrazone products from DCC can be directly isolated and characterized because the acyl hydrazone group is stable under acidic and physiological conditions. Acyl hydrazone-based DCC has been used to discover potent inhibitors for acetylcholinesterase,[4] *Bacillus subtilis* HPr kinase/phosphatase,[5] aspartic protease,[6] and β-tryptase.[7] The crystal structure of several acyl hydrazones in complexes with their protein targets have been reported.[8−12] On the other hand, the acyl hydrazone moiety has been recognized as a substructure of pan assay interference compounds (PAINS)[13] or causing false positives in bioassays.[14] Many biological activities have been associated with acyl hydrazones.[15] A literature search resulted in 11490 publications between 1993 and 2014 that discussed the biological activities of acyl hydrazones (see Figure S1 in the Supporting Information). However, few compounds were advanced to clinic studies. Two therapeutic drugs that do contain this functional group are nitrofurantoin and levosimendan. Therefore, it is urgent to evaluate the relationship between the biochemical and cell-based activities of acyl hydrazones and contemplate possible directions for inhibitor optimization. Herein, we report the biological evaluation and optimization of the inhibitors with this chemotype and the discovery of a selective inhibitor for the β-catenin/T-cell factor (Tcf) protein−protein interaction (PPI), an important downstream effector of canonical Wnt signaling.

Canonical Wnt signaling plays a critical role in regulating cell proliferation, differentiation, and cell−cell communication.[16,17] β-Catenin is a key mediator of this signaling pathway. The hyperactivation of canonical Wnt signaling promotes the transcription of cell proliferation, migration, and survival genes, such as *cyclin D1*,[18] *c-myc*[19] and *survivin*,[20] and is strongly associated with the initiation and progression of many cancers including colorectal carcinoma and fibroses. Cancer stem cells, which are resistant to conventional chemo- and radiotherapies and especially virulent, are also controlled by the hyperactivation of canonical Wnt signaling.[21−23] The formation of the β-catenin/Tcf complex in the cell nucleus is the penultimate step of canonical Wnt signaling. The overactivation of canonical Wnt signaling correlates with the formation of this complex.[24−26] Selective inhibition of the β-catenin/Tcf PPI represents an appealing therapeutic strategy.

The crystal structures of β-catenin in complexes with human Tcf4,[27−29] mouse Lef1,[30] and *Xenopus* Tcf3[31] have been

Received: February 8, 2015

DOI: 10.1021/acs.jmedchem.5b00223
J. Med. Chem. XXXX, XXX, XXX−XXX

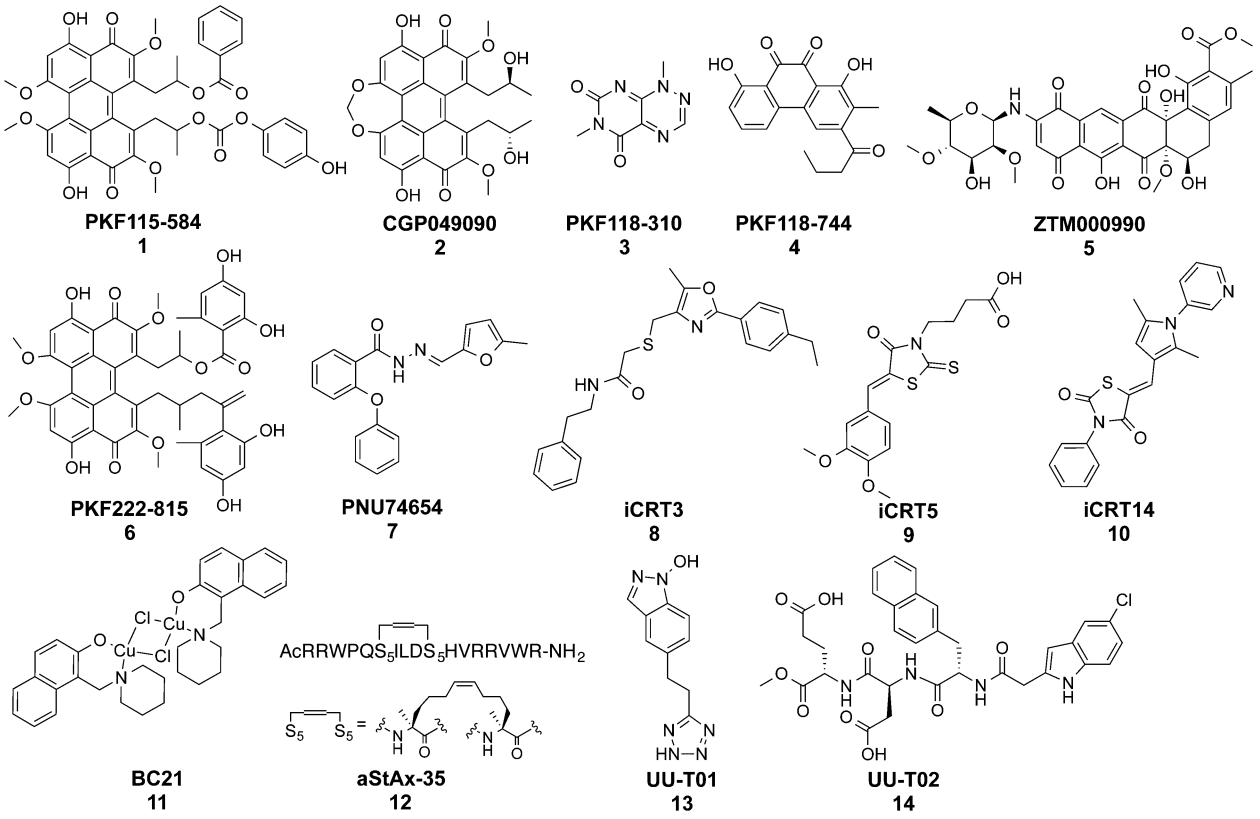

Figure 1. Chemical structures of the reported β-catenin/Tcf inhibitors. Compounds **1**, **2**, and **4**–**6** have quinone reactive groups (PAINS substructures 374, 376, and 377).[13] Compound **3** has a reactive redox recycler moiety, toxoflavin.[49] Compound **7** has an acyl hdrazone moiety (PAINS substructures 270 and 323).[13] Compounds **9** and **10** have the rhodanine-like groups (PAINS substructures 170 and 171).[13,52,53]

reported. These structures reveal a large protein−protein interface between β-catenin and Tcf [3500 Å^2 for β-catenin/Tcf4 PPIs (PDB id, 2GL7[29]) and 3700 Å^2 for β-catenin/Lef1 PPIs (PDB id, 3OUX[30])]. The crystallographic and biochemical studies also revealed three hot regions on β-catenin for the β-catenin/Tcf PPI:[27,31−35] hot region 1 includes K435 and K508 of β-catenin where D16 and E17 of Tcf4 binds, hot region 2 is K312 and K345 of β-catenin where E24 and E29 of Tcf4 bind using two alternative conformations,[27−29] and hot region 3 is a hydrophobic pockets lined with F253, I256, F293, A295, and I296. V44 and L48 of Tcf4 as well as axin[36] bind with this pocket. The crystal structures of β-catenin in complexes with cadherin[37] and adenomatous polyposis coli (APC)[38−40] were reported. A comparison of these crystal structures indicated that β-catenin used the same binding groove to bind cadherin (residues 819−876 of human E-cadherin) and APC (residues 1477−1519 of human APC 20-amino acid repeat 3, APC-R3; an APC repeat with the highest binding affinity). The central binding area of β-catenin was called the charge-button-recognition region (Supporting Information Figure S2).[31] One charge button is K312, and the other is K435. A conserved segment of Tcf/Lef, cadherin, and APC, Dx$\theta\theta$xΦx$_{2-7}$E, binds with this area. The biological assays confirm that the binding mode of Tcf/Lef, cadherin, and APC with β-catenin is mutually exclusive.[41] The β-catenin/cadherin PPI is essential for the integrity of epithelial junctions and the β-catenin/APC PPI is critical for β-catenin degradation in normal cells. The inhibitor that disrupts the β-catenin/cadherin PPI alters cell−cell adhesion, while the β-catenin/APC inhibitor overactivates Wnt signaling in normal cells and promotes new cancer formation. However, it is challenging to achieve inhibitor selectivity for β-catenin/Tcf over β-catenin/cadherin or β-catenin/APC PPIs because the dissociation constant (K_d) of the β-catenin/Tcf PPI is 7−10 nM[32,42,43] and much lower than those of the β-catenin/cadherin (K_d = 41−82 nM)[39,42,44] and β-catenin/APC (K_d = 0.6−3.1 μM for APC-R3[39,40,42,45,46]) PPIs.

Extensive efforts have been made to discover β-catenin/Tcf inhibitors, but few were successful. A high-throughput screening (HTS) on 52000 compounds identified six natural products as β-catenin/Tcf inhibitors, **1** (PKF115−584), **2** (CGP049090), **3** (PKF118−310), **4** (PKF118−744), **5** (ZTM000990), and **6** (PKF222−815) in Figure 1.[47] Compound **4** was used as a template for inhibitor optimization.[48] Nonetheless, all of these compounds have PAINS substructures (quinone[13] or toxoflavin[49]) and are frequent hits in biochemical assays. A combination of virtual and biophysical screening identified **7** (PNU-74654).[50] No further study was report for this compound. A compound screening by knocking down axin identified three inhibitors, **8** (iCRT3), **9** (iCRT5), and **10** (iCRT14) in Figure 1 for the Wnt effectors downstream of the axin-mediated degradation complex.[51] The pulldown assay revealed that **8** and **9** disrupted the β-catenin/Tcf PPI at high micromolar concentrations. Compounds **8**−**10** were reported to suppress the transcriptional activity of canonical Wnt signaling, downregulate Wnt/β-catenin-induced target genes, and inhibit the growth of colorectal cancer cells in vitro and in vivo. Compounds **9** and **10** contain a rhodanine PAINS substructure and are frequent hits in biochemical assays.[13,52,53] Compound **8** was reported to inhibit the β-catenin/androgen receptor interaction and androgen signaling.[54] A virtual screening using the Tcf4 D^{16}ELISF^{21} binding site of β-catenin

DOI: 10.1021/acs.jmedchem.5b00223
J. Med. Chem. XXXX, XXX, XXX−XXX

A

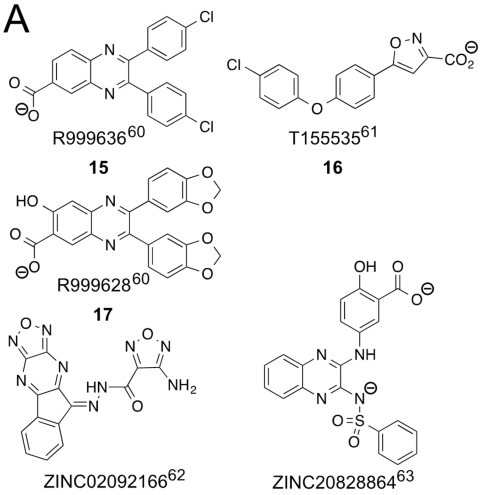

B

No.	K_i ± SD (μM) FP	AlphaScreen	No.	K_i ± SD (μM) FP	AlphaScreen
15	8.8 ± 0.48	13 ± 0.79	**3**[33,57]	5.8 ± 0.24	3.8 ± 0.45
16	77 ± 1.0	21 ± 0.76	**7**[33,57]	1.80 ± 0.72	n.d.
17	8.7 ± 1.0	12 ± 0.78	**8**[33,57]	370 ± 6.3	n.d.
18	5.8 ± 1.3	1.2 ± 0.39	**9**[33,57]	80 ± 4.2	n.d.
19	13 ± 2.5	n.d.	**10**[33,57]	54 ± 5.2	n.d.
1[33,57]	18 ± 2.1	n.a.	**13**[33]	3.1 ± 0.48	3.8 ± 0.45
2[33,57]	36 ± 4.4	5.9 ± 0.96	**14**[57]	1.4 ± 0.12	1.3 ± 0.56

C

No.	TOPFlash IC_{50} ± SD (μM) Wnt-activated HEK293	SW480
15	>1.0E2	n.d.
16	39 ± 5.6	n.d.
17	>1.0E2	n.d.
18	0.86 ± 0.51	0.71 ± 0.45
8	2.4 ± 0.52	1.1 ± 0.61
9	5.0 ± 0.50	4.0 ± 0.39

D

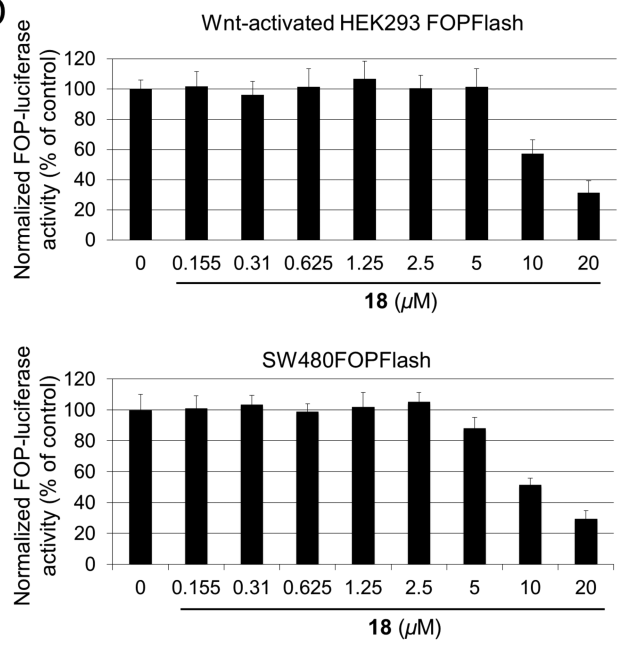

E

No.	IC_{50} ± SD (μM) SW480	HCT116	HT29
15	38 ± 1.1	22 ± 5.9	41 ± 1.0
16	>4.0E2	>4.0E2	430 ± 25
17	110 ± 21	250 ± 21	3.0E2 ± 18
18	0.85 ± 0.10	0.99 ± 0.13	1.1 ± 0.093
2	5.5 ± 1.3	1.2 ± 0.48	1.8 ± 0.13
9	240 ± 2.5	180 ± 2.9	290 ± 2.4

Figure 2. Results of compound screening. (A) Chemical structures of five compounds. Dianion **19** (ZINC20828864) was not further evaluated. (B) FP and AlphaScreen assay results. Each set of data is expressed as mean ± standard deviation (n = 3). Details are in Supporting Information Figure S3. (C) Wnt-responsive TOPFlash luciferase reporter assay results using pcDNA3.1−β-catenin transfected HEK293 cells and colorectal cancer SW480 cells. Each set of data is expressed as mean ± standard deviation (n = 3). Details are in Supporting Information Figure S4. (D) FOPFlash luciferase reporter assay results of **18** using pcDNA3.1−β-catenin transfected HEK293 cells and colorectal cancer SW480 cells. Each set of data is expressed as mean ± standard deviation (n = 3). (E) MTs assay results of β-catenin/Tcf inhibitors on the growth of colorectal cancer cells, SW480, HCT116, and HT29. Each set of data is expressed as mean ± standard deviation (n = 3). n.d., not determined. n.a., not applicable because **1** interferes with the AlphaScreen assay.[61]

identified an organocopper compound, **11** (BC21), that can disrupt the β-catenin/Tcf PPI, inhibit the transactivation of canonical Wnt signaling, down-regulate the expression of canonical Wnt target genes, and inhibit the growth of colorectal cancer cells.[55] The inhibitory selectivity of **11** for β-catenin/Tcf over β-catenin/cadherin and β-catenin/APC PPIs has not yet been reported. Hydrocarbon-stapled axin α-helix, **12** (aStAx-35) in Figure 1, was designed to bind hot region 3 of β-catenin and inhibit the β-catenin/Tcf PPI.[56] Axin is a scaffolding protein for β-catenin phosphorylation. The use of **12** might impair the degradation of β-catenin in normal cells. Recently, we reported targeting the Tcf4 G^{13}ANDE^{17} binding site to selectively inhibit the β-catenin/Tcf PPI.[57] A bioisosteric replacement technique was used to design new small organic molecules (fragments) to mimic the binding mode of Tcf4 D16 and E17, and **13** (UU-T01) was discovered.[33] In another series, human Tcf4 D16 and E17 were maintained in inhibitor scaffold. On the basis of the structure of Tcf4 peptide G^{13}ANDE^{17}, a peptidomimetic inhibitor, **14** (UU-T02) in Figure 1, was reported.[57] The diethyl ester of **14** was found to inhibit canonical Wnt signaling and the growth of colorectal cancer cells. This compound also exhibited cell-based selectivities for β-catenin/Tcf over β-catenin/cadherin and β-catenin/APC PPIs. Further structural optimization of **13** and **14** is under way.

RESULTS

Compound Screening to Discover Small-Molecule Inhibitors for the β-Catenin/Tcf Interaction. The homogeneous fluorescence polarization (FP) and AlphaScreen assays have been established to evaluate β-catenin/Tcf inhibitors.[58] In the FP assay, C-terminally fluorescein-labeled human Tcf4 (residues 7−51) and human β-catenin (residues 138−686) were used. After β-catenin and fluorescein-Tcf4 form a protein−protein complex, the fluorophore is attached to a high-molecular-weight protein complex (≥60 kDa) and has a low rotational speed when it is excited by plane-polarized light. The resulting emitted light is significantly polarized. When an

DOI: 10.1021/acs.jmedchem.5b00223
J. Med. Chem. XXXX, XXX, XXX−XXX

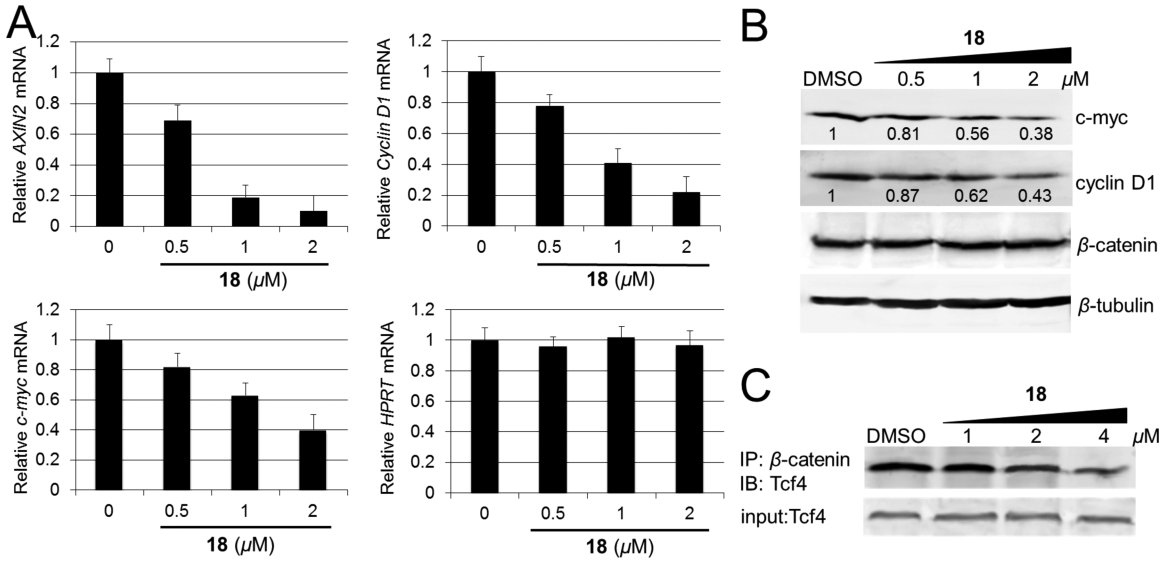

Figure 3. Cell-based characterization of **18**. (A) Quantitative real-time PCR study to determine the changes of mRNA expression of *AXIN2*, *cyclin D1*, *c-myc*, and *HPRT* in response to different concentrations of **18**. Each set of data is expressed as mean ± standard deviation (n = 3). (B) Western blot analysis to monitor the changes of protein expression of c-myc, cyclin D1, and β-catenin in response to different concentrations of **18**. β-Tubulin was used as an internal reference. (C) Coimmunoprecipitation experiment to evaluate the inhibitory effect of **18** on the β-catenin/Tcf association. IP, immunoprecipitation; IB, immunoblotting.

inhibitor completely disrupts the β-catenin/fluorescein-Tcf4 PPI, the fluorophore is only attached to Tcf4 (≤6 kDa), and the emitted light after excitation will be largely depolarized due to a high rotational speed of the fluorophore. AlphaScreen is a bead-based assay. The streptavidin-coated donor beads and the nickel-chelate acceptor beads are brought together through the interaction between *C*-terminally biotinylated human Tcf4 (residues 7−51) and *N*-terminally His_6-tagged human β-catenin (residues 138−686). On laser excitation at 680 nm, the photo sensitizers inside the donor beads convert ambient oxygen to a singlet oxygen state. Only when the donor and acceptor beads are brought within 200 nm can the singlet oxygen molecules diffuse to the acceptor beads, resulting in extensive emission at 570 nm. If the inhibitor completely disrupts the β-catenin/Tcf PPI, no luminescence signal will be observed. In this study, 269 Sigma-Aldrich carboxylic acids and sulfonamides, 90 LOPAC^{Pfizer} synthetic compounds, 24 compounds from the ZINC library, 117 natural products, and 1593 Diversity Set V compounds from the Developmental Therapeutics Program of NCI/NIH were screened. In the screening, carboxylic acids and acidic sulfonamides were prioritized because the acid-rich Tcf4 D^{16}ELISFKDE^{24} segment has been recognized as a key binding motif for the β-catenin/Tcf PPI. The compounds that displayed a K_i value ≤25 μM in either assay were kept for further evaluation. As shown in Figure 2A, four compounds exhibited reproducible and dose-dependent inhibitory activities in both assays. None of them were false positives in the AlphaScreen counter screen or aggregated as examined by the spin-down counter screen[59] and the dynamic light scattering experiments. None of these compounds had fluorescence interference in either assay. Figure 2B shows the results of the FP and AlphaScreen assays. Among them, compound **18** (ZINC02092166) is the most potent inhibitor. It is more potent than known inhibitors **1**, **2**, and **7**−**10** and comparable with **3**, **13**, and **14** in the parallel assays.[33,57]

To determine whether the above compounds inhibit the transactivation of canonical Wnt signaling, Wnt-responsive luciferase reporter assays were performed.[64] As shown in Figure 2C, compound **16** inhibited the TOPFlash luciferase (a luciferase reporter with eight wild-type Tcf binding sites) activity in Wnt-activated HEK293 cells. Compound **18** inhibited the TOPFlash luciferase activity in both tested cell lines, pcDNA3.1−β-catenin transfected HEK293, and colorectal cancer SW480 by dose-dependent manners with the IC_{50} values of 0.86 ± 0.51 and 0.71 ± 0.45 μM. Compounds **8** and **9**, which were identified by the highly sensitive luciferase reporter (Super 16× TOPFlash) assay,[51] were used as the reference inhibitors for comparison. Compound **18** also inhibited the FOPFlash luciferase (a luciferase reporter with eight mutant Tcf binding sites) activity at the concentrations ≥5 μM (Figure 2D), indicating off-target effects at high concentrations. It was worth noting that **8** and **9** also inhibited the FOPFlash luciferase reporter activity, as shown in Supporting Information Figure S4.

The MTs cell viability assay was performed to assess the effects of these compounds on the growth of colorectal cancer cell lines, SW480, HCT116, and HT29. These cancer cell lines were chosen based on their known dependence on the β-catenin/Tcf PPI for growth and survival. SW480 and HT29 cells harbor the deletions of APC, whereas HCT116 cells harbor a mutation on β-catenin that blocks β-catenin phosphorylation and ubiquitination.[65,66] The MTs assay results indicated that **15** inhibited the growth of SW480, HCT116, and HT29 cells with the IC_{50} values of 38 ± 1.1, 22 ± 5.9, and 41 ± 1.0 μM. Compound **18** inhibited the growth of SW480, HCT116, and HT29 cells with the IC_{50} values of 0.85 ± 0.10, 0.99 ± 0.13, and 1.1 ± 0.093 μM, respectively (Figure 2E).

Effects of 18 on the Expression of Wnt/β-Catenin Target Genes and the Co-immunoprecipitation Study. *AXIN2* is a specific target gene for the canonical Wnt signaling pathway.[67] *Cyclin D1* and *c-myc* are two Wnt target genes that drive cancer progression including in SW480 cells.[18,19] The quantitative real-time PCR study indicated that **18** down-regulated the expression of *AXIN2*, *cyclin D1*, and *c-myc* in a

DOI: 10.1021/acs.jmedchem.5b00223
J. Med. Chem. XXXX, XXX, XXX−XXX

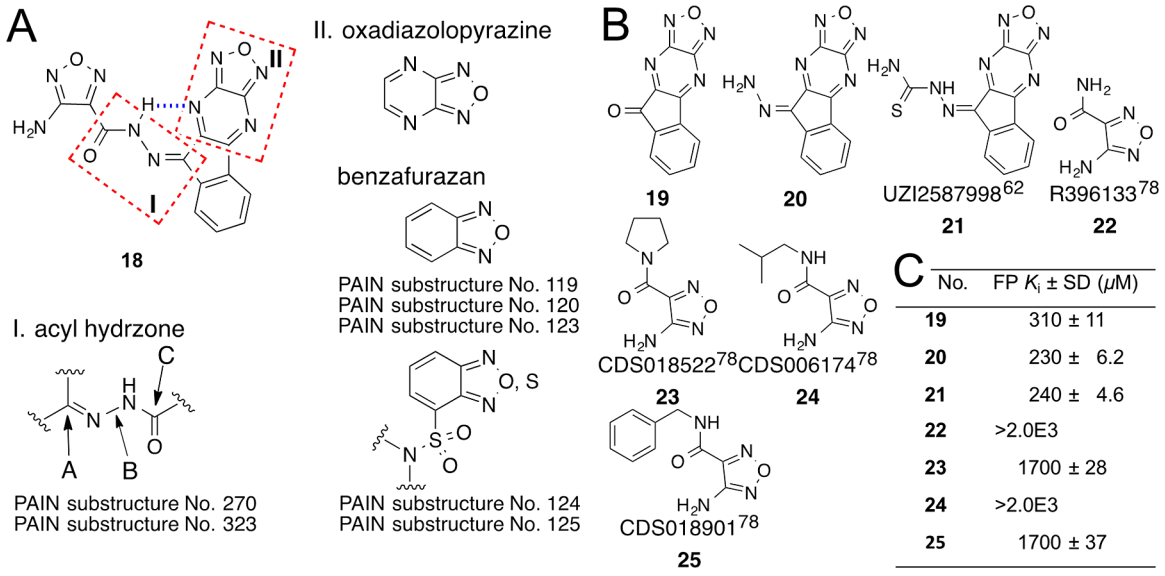

Figure 4. Structural analysis of **18**. (A) Potential reactive sites of **18**. The intramolecular H-bond between the oxadiazolopyrazine moiety and acyl hydrazone is shown blue. (B) Chemical structures of **19**–**25**. (C) FP assay results of **19**–**25**. Each set of data is expressed as mean ± standard deviation (n = 3). Details are in Supporting Information Figure S5.

dose-dependent manner in SW480 cells, as shown in Figure 3A. More than 50% of mRNA expression was inhibited at a dose of 2 μM. Compound **18** did not affect the expression of housekeeping gene *HPRT*. The protein expression levels of cyclin D1, c-myc, and β-catenin in SW480 cells were examined by the Western blot analysis (Figure 3B). The expression of proteins cyclin D1 and c-myc were significantly reduced after the treatment with **18**. Compound **18** did not reduce the expression level of β-catenin, indicating that it does not inhibit the β-catenin degradation pathways. A coimmunoprecipitation experiment was performed to evaluate the inhibitory potency of **18** in a cellular context. As shown in Figure 3C, compound **18** inhibits the β-catenin/Tcf PPI in a dose-dependent manner in SW480 cells.

Fragmentation of Compound 18. Compound **18** exhibited a higher inhibitory potency in cell-based studies than in the FP and AlphaScreen assays and inhibited the FOPFlash luciferase activity. This brought the concern that **18** had off-target effects. An analysis of the structure of **18** indicated two functional groups that might be problematic (Figure 4A). One is the acyl hydrazone moiety, which has been identified as a PAINS substructure. Out of three vulnerable sites in acyl hydrazone, site A, the nucleophilic imine carbon atom, is most reactive and susceptible to nucleophilic attack. A similar site in hydrazones has been reported causing frequent hits in biochemical assays.[68,69] The N–N single bond is an "undesirable" substructure due to the reactivity to nucleophiles.[70] In any case, site B of **18** is located in an electron-deficient environment and unlikely to be reactive. Site C, the amide carbon atom, is more stable than sites A and B. The second is the oxadiazolopyrazine ring. No false positive reactivity is associated with this functional group. A related substructure, benzafurazan, has been reported as a PAINS substructure.[13,71–73] However, the reactivity of benzafurazan with singlet oxygen[74] and nucleophiles[75] is caused by the fused benzene ring, which is absent in **18**. The hydrophilic nature of the oxadiazolopyrazine moiety and the low polarizability of the tetracyclic ring make **18** unlikely to be a DNA intercalator.[76,77] It is worth noting that an intramolecular H-bond between the nitrogen atom of the oxadiazolopyrazine moiety and the NH group of acyl hydrazone may stabilize the structure of **18**, as shown in Figure 4A.

Because the nucleophilic imine carbon atom of **18** was recognized problematic, a fragmentation of **18** was conducted. As shown in Figure 4C, compounds **19**–**21**, **23**, and **25** exhibited some inhibitory activities for the disruption of the β-catenin/Tcf PPI but were much lower than **18**. The synthesis of **19** and **20** is shown in Scheme 1. The condensation reaction

Scheme 1

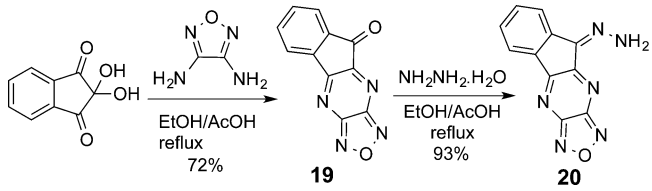

between ninhydrin and 1,2,5-oxadiazole-3,4-diamine generated **19**, which was converted to **20** through a condensation with hydrazine hydrate in glacial acid.

Structure–Activity Relationship of the Derivatives of 18. Further optimization started with the resynthesis of **18** to examine the chemical structure. As shown in Scheme 2, 4-amino-1,2,5-oxadiazole-3-carboxylic acid was refluxed in methanol under acidic conditions that afforded methyl ester **39**, which was converted to **40** by hydrazinolysis. Compound **18** was obtained through a condensation reaction between **19** and **40**. The FP and AlphaScreen assays indicated that the resynthesized **18** had a similar biological activity as that observed in commercially available **18** (Figure 2B and Figure 5E). The AutoDock Vina[79] blind docking study was performed to explore the possible binding pockets in β-catenin for **18**. The result predicted that **18** preferentially bound to hot region 1 (AutoDock Vina scores were −8.4, −4.6, and −3.7 kcal/mol for hot regions 1, 2, and 3, respectively). The Glide,[80] AutoDock,[81] and AutoDock Vina docking studies predicted one recurring binding conformation of **18** in β-catenin, as shown in Figure

DOI: 10.1021/acs.jmedchem.5b00223
J. Med. Chem. XXXX, XXX, XXX–XXX

Scheme 2

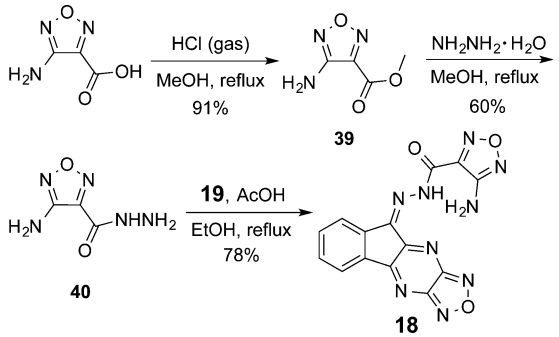

5B: the 4-amino-1,2,5-oxadiazole ring was predicted to form H-bonds with the side chain amino group of K435 and the backbone NH group of N430, the amide carbonyl group of **18** was predicted to form H-bonds with the side chain amide group of N516 and the hydroxyl group of S473, the tetracyclic ring was predicted to form a cation−π interaction with the positively charged gaunidino group of R469, two nitrogen atoms of the oxadiazolopyrazine ring formed H-bonds with K508, and the benzene ring was predicted to locate in hydrophobic pocket B. Crystallographic analyses indicated that R469, V511, and I569 did not interfere with the β-catenin/Tcf PPI. Three mutants, R469A, V511S, and V511S/I569S, were made.[33,57] Native gel electrophoresis, thermal shift, and CD experiments confirmed the homogeneity, the thermal stability, and the secondary structure integrity of all purified proteins. The FP saturation binding assays demonstrated that V511S, V511S/I516S, and R469A of β-catenin had the same apparent K_d values as wild-type β-catenin when binding with wild-type Tcf4, as shown in Supporting Information Figure S7. The FP competitive inhibition assay was performed to evaluate the roles of these three residues in inhibitor binding. The K_i value of the resynthesized **18** for wild-type β-catenin/Tcf4 interactions was 7.0 ± 4.1 μM. The K_i values of the resynthesized **18** for β-catenin V511S/Tcf4 and β-catenin V511S/I569S double mutant/Tcf4 interactions were 2.0×10^1 ± 1.7 and 36 ± 3.1 μM, respectively. It suggests that a change of pocket B from hydrophobic to hydrophilic greatly reduces the potency of **18**. The K_i value of the resynthesized **18** for β-catenin R469A/Tcf4 interactions was 46 ± 4.3 μM, indicating the role of R469 in inhibitor binding.

As shown in Figure 5A, the tetracylic ring of **18** is not aromatic. Instead, it contains two aromatic substructures, oxadiazolopyrazine and benzene. The imine carbon atom is located at the dibenzylic position and potentially reactive. A

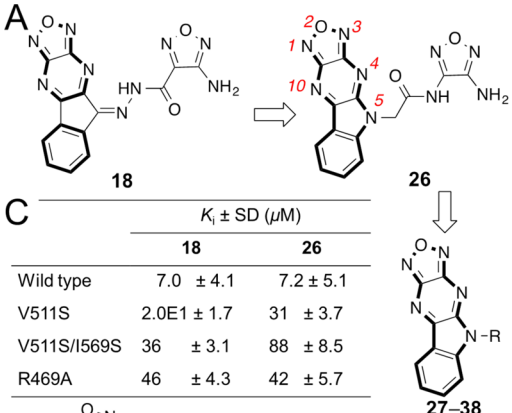

C

	K_i ± SD (μM)	
	18	**26**
Wild type	7.0 ± 4.1	7.2 ± 5.1
V511S	2.0E1 ± 1.7	31 ± 3.7
V511S/I569S	36 ± 3.1	88 ± 8.5
R469A	46 ± 4.3	42 ± 5.7

D

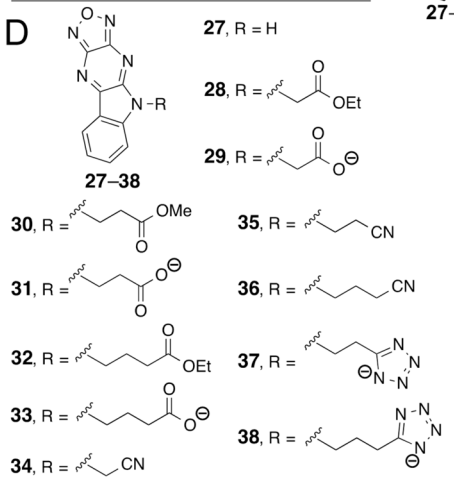

E

No.	K_i ± SD (μM) FP	AlphaScreen
18	7.0 ± 4.1	1.7 ± 0.31
26	7.2 ± 5.1	2.7 ± 0.45
27	280 ± 12	120 ± 8.7
28	150 ± 7.8	63 ± 5.2
29	5.8 ± 1.5	4.1 ± 0.53
30	1.0E2 ± 9.1	1.0E2 ± 2.5
31	11 ± 3.6	3.3 ± 0.56
32	120 ± 41	52 ± 2.3
33	3.4 ± 1.2	1.0 ± 0.13
34	240 ± 14	>130
35	47 ± 5.0	39 ± 2.0
36	160 ± 8.9	120 ± 4.2
37	17 ± 1.8	18 ± 2.2
38	51 ± 13	74 ± 2.3

F

No.	IC_{50} ± SD (μM) β-catenin/Tcf4	β-catenin/E-cadherin	β-catenin/APC-R3
18	3.0E1 ± 18	6.0E1 ± 8.0	52 ± 15
26	31 ± 21	550 ± 58	630 ± 19
29	25 ± 4.9	280 ± 24	450 ± 28
31	48 ± 13	580 ± 33	790 ± 29
33	15 ± 5.3	170 ± 26	340 ± 25
37	76 ± 7.8	770 ± 38	850 ± 29
1[60]	77 ± 9.3	38 ± 1.6	110 ± 0.58
2[60]	150 ± 19	41 ± 1.6	130 ± 0.38
3[60]	3.0E1 ± 1.5	34 ± 0.75	340 ± 0.70
13[60]	13 ± 2.4	3.0E2 ± 1.3	350 ± 1.9
14[57]	6.3 ± 0.76	680 ± 6.8	210 ± 3.0

Figure 5. Inhibitor optimization for **18**. (A) Strategy for inhibitor optimization. The numbering of the heteroatoms in the tetracyclic ring is shown. (B) Glide docking model of **18** with β-catenin. A stick model is shown in Supporting Information Figure S6. (C) Results of the site-directed mutagenesis studies of the resynthesized **18** and **26**. Each set of data is expressed as mean ± standard deviation (n = 3). Details are in Supporting Information Figures S7 and S10. (D) Chemical structures of **27**−**38**. (E) FP and AlphaScreen assay results for the resynthesized **18** and **26**−**38**. Each set of data is expressed as mean ± standard deviation (n = 3). Details are in Supporting Information Figures S8 and S9. (F) FP selectivity assay results for the resynthesized **18**, **26**, **29**, **31**, **33**, and **37**. Each set of data is expressed as mean ± standard deviation (n = 3). Details are in Supporting Information Figure S11.

DOI: 10.1021/acs.jmedchem.5b00223
J. Med. Chem. XXXX, XXX, XXX−XXX

Scheme 3

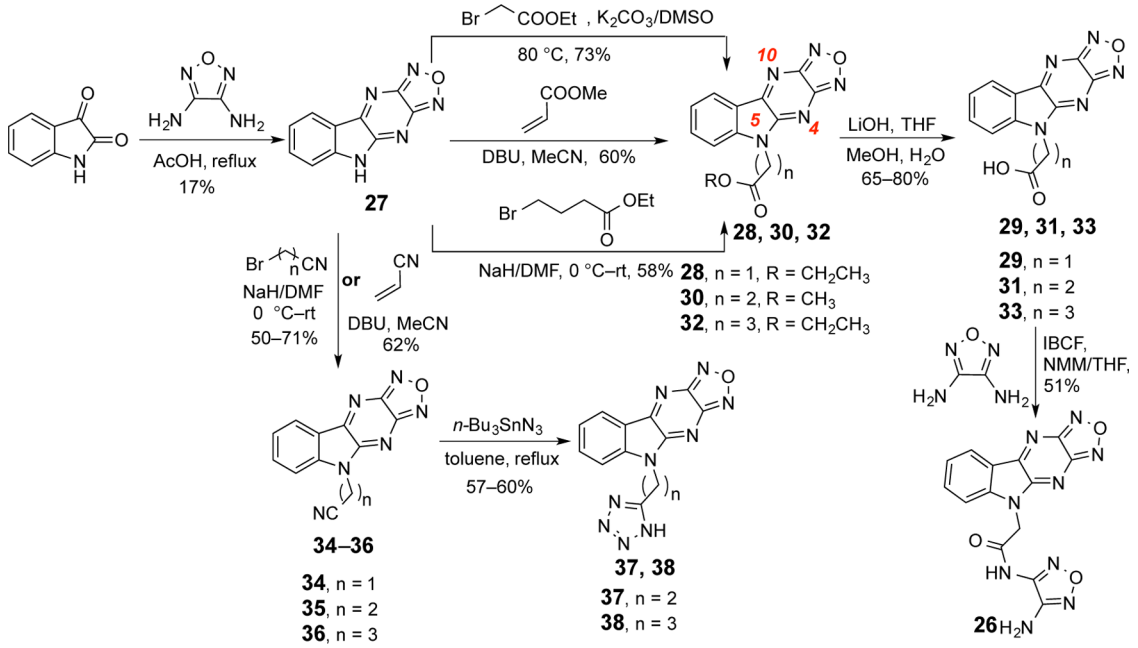

nitrogen atom was used to replace this carbon atom. This modification converts the tetracyclic ring into an aromatic system, increases its chemical stability, and maintains the cation−π interaction with R469. The hydrazide substructure of **18** was changed to an amide, and **26** was designed. The synthesis of **26** is shown in Scheme 3. Condensation of isatin with 1,2,5-oxadiazole-3,4-diamine afforded **27** in low yield (17%). In agreement with the results described previously,[82,83] the alkylation in an alkaline medium gave N^5-substituted derivative **28** as the major product. No N^4 or N^{10}-alkylated byproducts were isolated. The ester hydrolysis/peptide bond coupling sequence generated **26** with moderate yield. The FP and AlphaScreen assays indicated that the inhibitory activity of **26** was similar to that of **18** (Figure 5E). The site-directed mutagenesis study indicated that V511, I569, and R469 are important for the inhibitory activity of **26** (Figure 5C).

Compounds **27**−**38** were designed to evaluate the contribution of the 4-amino-1,2,5-oxadiazole ring to inhibitor potency (Figure 5D). The synthesis is also shown in Scheme 3. An aza-Michael addition reaction afforded **30**. The nucleophilic substitution reactions in alkaline medium generated **32**. The hydrolysis of the methyl or ethyl ester afforded **29**, **31**, and **33**. The nucleophilic substitution of **27** with brominated alkylnitriles or the aza-Michael addition reaction with acrylonitrile generated **34**−**36**. The [2 + 3] cycloaddition reaction of **35** and **36** produced **37** and **38** with moderate yield. Without a side chain, compound **27** showed poor inhibitory potency. Compounds **29**, **31**, and **33**, in which carboxylic acid side chains were predicted to form charge−charge interactions with charge button K435, exhibited a much higher inhibitory potency. Their methyl or ethyl esters (compounds **28**, **30**, and **32**) were poor inhibitors. The nitrile derivatives, **34**−**36**, also exhibited poor inhibitory activity. When the nitrile group was converted to a tetrazole moiety (compounds **37** and **38**), a bioisostere of carboxylic acid, the inhibitory potency was improved. Among these inhibitors, compound **33** exhibited the highest inhibitory potency for the β-catenin/Tcf PPI in the biochemical assays (Figure 5E).

The FP selectivity assay[61] was used to quantify inhibitor selectivities between β-catenin/Tcf, β-catenin/cadherin, and β-catenin/APC PPIs. As shown in Figure 5F, compounds **26**, **29**, **31**, **33**, and **37** show dual selectivity for β-catenin/Tcf over β-catenin/cadherin and β-catenin/APC PPIs. Compound **18** exhibits marginal selectivity among these three PPIs, again implying off-target effects. The selectivity of known β-catenin/Tcf inhibitors were also listed for comparison.[57,61] It is worth noting that the data in Figure 5F reflect inhibitory potency under the assay conditions used. More analysis will be required to fully understand the selectivity of the inhibitors for β-catenin/Tcf over β-catenin/cadherin and β-catenin/APC PPIs.

Biological Characterization of the Derivatives of 18 as β-Catenin/Tcf Inhibitors. The Glide docking mode of **33** and **37** with β-catenin is shown in Figure 6A,B. The tetracyclic ring of **33** and **37** was predicted to form a cation−π interaction with the positively charged gaunidino group of R469. The benzene moiety of the tetracylic ring was predicted to locate in hydrophobic pocket B. Two nitrogen atoms of the oxadiazolopyrazine ring of **33** and **37** were predicted to form H-bonds with K508. The carboxylic group of **33** and the tetrazole ring of **37** were predicted to form a salt bridge with K435 and H-bonds with the backbone NH group of N470 and the hydroxyl group of S473. Site-directed mutagenesis was performed to evaluate the contribution of three residues, R469, V511, and I569, to inhibitor potency. As shown in Figure 6C, the K_i value of **33** for the wild-type β-catenin/wild-type Tcf4 interaction was 3.4 ± 3.3 μM. The K_i values of **33** for β-catenin V511S mutant/wild-type Tcf4, β-catenin V511S/I569S double mutant/wild-typeTcf4, and β-catenin R469A mutant/wild-type Tcf4 interactions were 17 ± 1.4, 59 ± 4.2, and 42 ± 3.5 μM, respectively. The same trend was also observed for **37**. These results suggest the importance of the hydrophobicity in pocket B and the positively charged side chain of β-catenin R469 for the inhibitory potency of **33** and **37**.

The Wnt-responsive luciferase reporter assay was performed with pcDNA3.1−β-catenin transfected HEK293 cells for **26**, **30**, **32**, **33**, and **37**. Compounds **26**, **30**, **32**, and **33** did not

DOI: 10.1021/acs.jmedchem.5b00223
J. Med. Chem. XXXX, XXX, XXX−XXX

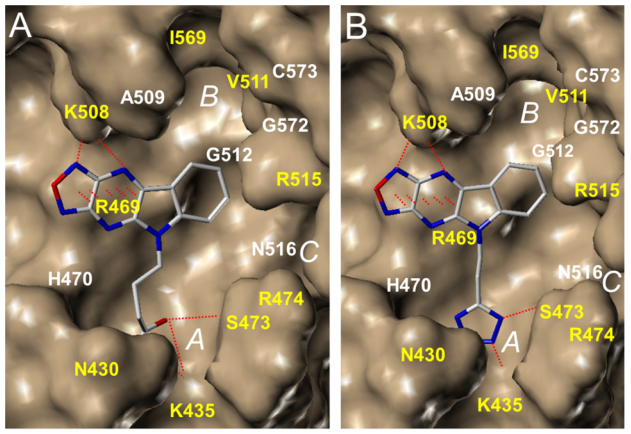

C

No.	K_i ± SD (μM), β-catenin wild type	V511S	V511S/I569S	R469A
33	3.4 ± 3.3	17 ± 1.4	59 ± 4.2	42 ± 3.5
37	17 ± 5.6	53 ± 4.1	180 ± 6.4	52 ± 7.5

Figure 6. Biochemical characterization of **33** and **37** as β-catenin/Tcf inhibitors. (A,B) Glide docking models of **33** and **37** with β-catenin. The stick models are shown in Supporting Information Figure S12. (C) Results of the FP competitive inhibition assay to determine the effects of site-directed mutagenesis studies for **33** and **37**. Each set of data is expressed as mean ± standard deviation (n = 3). Details are in Supporting Information Figure S13.

inhibit the transactivation of canonical Wnt signaling presumably due to low cell permeability. However, compound **37** suppressed the TOPFlash luciferase activity in a dose-dependent manner, as shown in Figures 7A. This compound did not affect the FOPFlash luciferase activity even at 200 μM (Figure 7B). Compound **37** also down-regulated the expression of Wnt-specific target gene *AXIN2* in a dose-dependent manner in SW480 cells (Figure 7C). The same trend was also observed for the inhibition of two other target genes, *cyclin D1* and *c-myc*. This compound did not affect the expression of house-keeping gene *HPRT* in the parallel assay. The MTs cell viability assay was performed to assess the inhibitory effects of **26**, **30**, **32**, **33**, **35**, and **37** on the growth of colorectal cell lines SW480 and HCT116. Compounds **26**, **30**, **32**, and **33** did not exhibit the inhibitory activities. Compound **35** inhibited the growth of SW480 but not HCT116 cells. Compound **37** inhibited the growth of Wnt-activated cancer cells with the IC_{50} values of $2.0 \times 10^1 \pm 4.1$ μM and 31 ± 6.0 μM for SW480 and HCT116 cells, respectively, as shown in Figure 7D.

DISCUSSION

Dynamic combinatorial chemistry is a powerful in situ fragment assembly technique for the discovery of bioactive small molecules.[84] The reaction to form an acyl hydrazone moiety has been preferred in DCC because it offers a favorable kinetic and thermodynamic balance for product formation. The acyl hydrazone structure has both H-bond donor and acceptor sites for molecular recognition and improves the success rate of the DCC experiments. Along with the application of the acyl hydrazone moiety in DCC, many biologically active compounds that contain an acyl hydrazone moiety have been reported, but few were advanced to the late stage of drug development. Hence, it is necessary to evaluate the biochemical and cell-based activities of acyl hydrazones in parallel and design possible strategies for inhibitor optimization.

The hyperactivation of the canonical Wnt signaling pathway causes the growth and progression of many cancers and fibroses. Human cancers also have a subpopulation of cancer stem cells that drive tumor growth, seed metastasis, and induce cancer recurrence after remission. They must be eradicated to achieve a durable cancer cure. Canonical Wnt signaling is highly activated in cancer stem cells. The formation of the β-catenin/Tcf complex in the cell nucleus is the key downstream effector

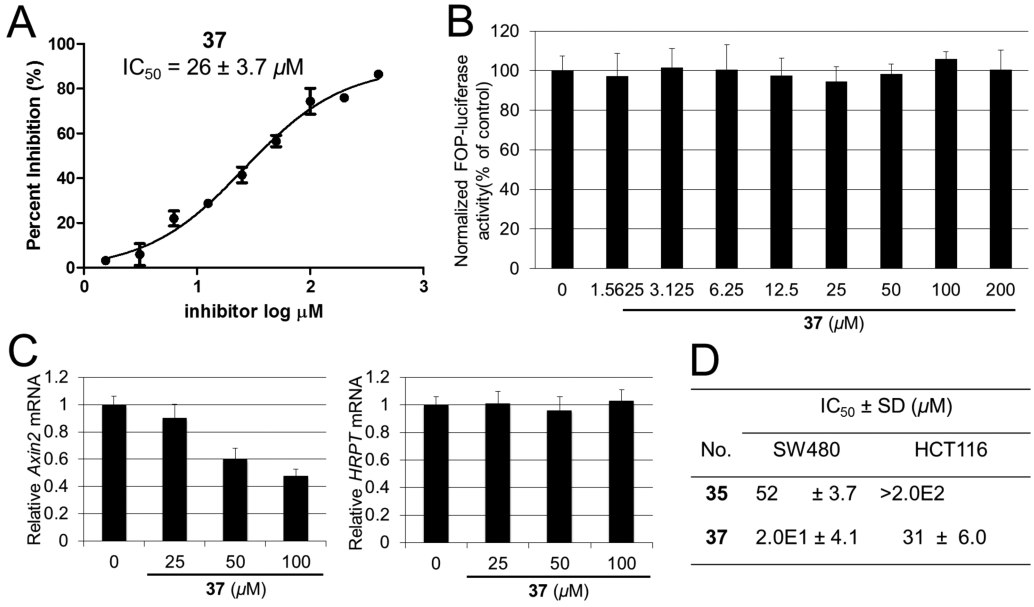

D

No.	IC_{50} ± SD (μM) SW480	HCT116
35	52 ± 3.7	>2.0E2
37	2.0E1 ± 4.1	31 ± 6.0

Figure 7. Cell-based characterization of **37** as a β-catenin/Tcf inhibitor. (A,B) TOPFlash and FOPFlash luciferase reporter assay results of **37** using pcDNA3.1−β-catenin transfected HEK293 cells. The data are expressed as mean ± standard deviation (n = 3). (C) Quantitative real time PCR study to determine the changes of mRNA expression of *AXIN2* and *HPRT* in response to different concentrations of **37**. Each set of data is expressed as mean ± standard deviation (n = 3). (D) MTs assay to monitor the inhibitory effects of **35** and **37** on the growth of colorectal cancer cells SW480 and HCT116. Each set of data is expressed as mean ± standard deviation (n = 3).

DOI: 10.1021/acs.jmedchem.5b00223
J. Med. Chem. XXXX, XXX, XXX−XXX

of canonical Wnt signaling. The selective inhibition of the β-catenin/Tcf PPI represents an appealing therapeutic target. β-Catenin and Tcf have a large contacting surface area and a tight binding affinity. This PPI target has been challenging for compound screening campaigns. In our screening using the homogeneous AlphaScreen and FP assays, compound **18** that contains an acyl hydrazone group was identified as a β-catenin/Tcf inhibitor. Its inhibitory activity was further confirmed by the cell-based coimmunoprecipitation study. This compound blocks the transactivation of canonical Wnt signaling, suppresses the expression of Wnt/β-catenin target genes, and inhibits the growth of colorectal cancer cells in dose-dependent manners. The cell-based activities of **18** were higher than that from the biochemical assays and **18** inhibited the FOPFlash luciferase activity, suggesting off-target effects.

The blind docking study predicted that **18** bound the Tcf4 $G^{13}ANDE^{17}$ binding site of β-catenin. The site-directed mutagenesis experiments indicated that the residues that are lined with the Tcf4 $G^{13}ANDE^{17}$ binding site were sensitive to inhibitor binding. The previous crystallographic and biochemical studies have demonstrated that β-catenin used the same binding groove to interact with Tcf, cadherin, and APC with the central binding area called the charge-button-recognition region. Our study concluded that three hot regions of β-catenin contributed differently to the β-catenin/Tcf, β-catenin/cadherin, and β-catenin/APC PPIs.[33,57] Hot region 1 of β-catenin is more important for the β-catenin/Tcf PPI than for the other two PPIs. The peptidomimetic inhibitor of Tcf4 $G^{13}ANDE^{17}$ exhibits dual selectivity for β-catenin/Tcf over β-catenin/cadherin and β-catenin/APC PPIs.[57] The result that the Tcf4 $G^{13}ANDE^{17}$ binding site of β-catenin was sensitive to the inhibitory activity of **18** intrigued us to conduct a structure-based optimization to replace the potential reactive moiety in **18**, albeit that **18** exhibited a low selectivity between these three protein−protein complexes. Through the replacement of the acyl hydrazone moiety with a chemically stable substructure, compounds **26** and **33** were discovered to exhibit comparable inhibitory activities as **18**, however, they showed much higher selectivity for β-catenin/Tcf over β-catenin/cadherin and β-catenin/APC PPIs. The results of the site-directed mutagenesis study and the SAR analysis were in consistent with the proposed binding modes. Compounds **26**, **32**, and **33** did not exhibit cell-based activity. Further optimization resulted in **37** that was active in both biochemical and cell-based assays. This compound selectively inhibited the transactivation of canonical Wnt signaling.

CONCLUSION

Most PPIs for which potent small-molecule inhibitors are discovered have a contacting surface area of <2500 $Å^2$. The discovery of small-molecule inhibitors for the PPI that has a larger contacting surface areas is challenging.[85] It is even more challenging when the same protein interface is used to bind multiple different protein partners. The β-catenin/Tcf PPI represents such a case. β-Catenin/Tcf, β-catenin/cadherin, and β-catenin/APC PPIs share the same surface area of β-catenin. Furthermore, β-catenin and Tcf have a large contacting surface area (3500 $Å^2$ for β-catenin/Tcf4 PPIs, and 3700 $Å^2$ for β-catenin/Lef1 PPIs) and a strong binding affinity (K_d = 7−10 nM for β-catenin/Tcf4 PPIs). Low hit rates have been associated with compound screening efforts for this target. Our screening based on the homogeneous FP and AlphaScreen assays identified a small molecule, **18**, that can disrupt the β-catenin/Tcf PPI in both biochemical and cell-based assays, inhibit the transactivation of canonical Wnt signaling, and down-regulate the expression of the target genes that are specific for the canonical Wnt signaling pathway. However, this compound exhibits a higher inhibitory activity in cell-based assays than biochemical assays and inhibits the FOPFlash luciferase activity. A close examination identified that the acyl hydrazone moiety in **18** is reactive and might cause off-target effects. On the basis of the proposed binding mode, compound **18** was optimized into chemically stable derivatives. Compounds **26**, **29**, **31**, **33**, and **37** were found to exhibit dual inhibitory selectivity. The binding mode of these inhibitors with β-catenin was characterized by the site-directed mutagenesis study and the SAR analysis. *These results again indicated that targeting the Tcf4 $G^{13}ANDE^{17}$ binding site of β-catenin with small molecules can selectively inhibit the β-catenin/Tcf PPI.*[57] Compound **37** was found to block the transactivation of canonical Wnt signaling, suppress the expression of Wnt-specific target genes, and inhibit the growth of cancer cells. Its cell-based inhibitory activities are aligned with that from the biochemical assays.

For many PPI targets, it is difficult to discover PAINS-free inhibitors by either high-throughput screening or fragment-based screening. This study provides a new path to approaching chemically stable hits through the optimization of the acyl hydrazone moiety after the initial hit is discovered. The new chemically stable and selective β-catenin/Tcf inhibitors with a new scaffold reported in this study provide an excellent starting point to generate more potent and more selective inhibitors specific for the β-catenin/Tcf PPI. Indeed, the inhibitory selectivities of new derivatives for β-catenin/Tcf over β-catenin/cadherin and β-catenin/APC PPIs are still relatively low. However, in consideration that the K_d value of the β-catenin/Tcf PPI is much lower than that for the β-catenin/cadherin and β-catenin/APC PPIs, the inhibitory selectivities of **26**, **29**, **31**, **33**, and **37** are significant. Further, the selectivity profile of the inhibitors for the β-catenin/Tcf PPI over the β-catenin/cadherin and β-catenin/APC PPIs can be optimized. Pockets B and C in parts A and B of Figure 6 are only important for the β-catenin/Tcf PPI. The modification of the inhibitors by better occupying pockets B and C would lead to new inhibitors with better potency and selectivity.

EXPERIMENTAL SECTION

Protein Expression and Purification. β-Catenin V511S, V511S/I569S, and R469A mutants have been made previously.[33,57] Wild-type β-catenin and its mutants (residues 138−686) were cloned into a pET-28b vector carrying a *C*-terminal 6× histidine (Novagen) or a pEHISTEV vector carrying an *N*-terminal 6× histidine (from Dr. Hanting Liu, St. Andrew University, UK) and transformed into *Escherichia coli* BL21 DE3 (Novagen). Cells were cultured in LB medium with 30 μg/mL kanamycin until the OD_{600} was approximately 0.8, and then protein expression was induced with 400 μM of IPTG at 20 °C overnight. Cells were lysed by sonication. The proteins were purified by Ni-NTA affinity chromatography (30210, Qiagen) and dialyzed against a buffer containing 20 mM of Tris (pH 8.8), 100 mM NaCl, 10% glycerol, and 3 mM DTT. The purity of β-catenin was set to >95% as determined by SDS-PAGE gel analysis. Native non-denaturing gel electrophoresis experiment and the thermal-shift assay on an iCycler iQ real-time detection system (Bio-Rad) were performed for each purified protein. In the thermal shift assay, protein unfolding was evaluated through measuring the fluorescence changes of fluorescent dye Sypro Orange with purified β-catenin proteins. A temperature increment of 1 °C/min was applied to monitor protein stability and detect protein aggregation. CD spectra were measured on

DOI: 10.1021/acs.jmedchem.5b00223
J. Med. Chem. XXXX, XXX, XXX−XXX

a J-815 spectropolarimeter (Jasco). All spectra were recorded using a 1 mm path-length quartz cell. The CD spectra were averaged over three scans, and the wavelength was scanned from 260 to 190 nm in steps of 1 nm. All spectra were recorded at room temperature, and the baseline was corrected by subtracting the CD spectra of a blank control containing all of the substances except protein. Samples were prepared at a concentration around 1−5 μM in a buffer of 10 mM potassium phosphate and 100 mM potassium fluoride at pH 7.0 to ensure that the transmission of light through the sample was not restricted. All proteins were stable, and no aggregation was observed under storage or assay conditions. Proteins were aliquoted and stored at −80 °C. *C*-Terminally biotinylated human Tcf4 (residues 7−51), *C*-terminally fluorescein-labeled human Tcf4 (residues 7−51), *C*-terminally fluorescein-labeled human E-cadherin (residues 819−873), and *C*-terminally fluorescein-labeled human APC-R3 (residues 1477−1519) were synthesized by InnoPep, Inc. (http://www.innopep.com/) and HPLC purified with purity >95%. The structures were validated by LC/MS (liquid chromatography/mass spectrometry). The peptide sequences are shown in Supporting Information Figure S14.

FP and AlphaScreen Assays. The procedures for the FP and AlphaScreen competitive inhibition assays have been described previously[58,61] Briefly, all of the tested compounds were prepared as 10 mM DMSO stocks. In the primary screen, the concentrations of the compounds and DMSO were set to 50 μM and 1% (v/v). Only the compounds which AlphaScreen or FP signal decreases were greater than 50% in the single-point β-catenin/Tcf assay were evaluated by counter screen. Compounds that were confirmed active in the competitive inhibition assay and inactive in the counter screen were further evaluated with the dose−response relationship. In the FP competitive inhibition assay, 10 nM human β-catenin and 2.5 nM of *C*-terminally fluorescein-labeled human Tcf4 were incubated in an assay buffer of 137 mM NaCl, 2.7 mM KCl, 10 mM Na_2HPO_4, 2 mM KH_2PO_4, 100 μg/mL of bovine γ-globulin, and 0.01% Triton-X100 for 15 min at 4 °C. Bovine γ-globulin and Triton-X100 were included in the assay buffer to decrease the likelihood of compound acting by aggregate formation. Different concentrations of the tested compounds in the assay buffer were added to each test plate to make a final volume of 100 μL. Each assay plate was covered black and gently mixed on an orbital shaker at 4 °C for 1.5 h to reach equilibrium before the polarization values were read. The IC_{50} value was determined by nonlinear least-squares analysis of GraphPad Prism 5.0. The K_i values were derived.[86] Experiments were performed in triplicate and carried out in the presence of 1% DMSO. For the β-catenin/E-cadherin inhibition assay, 150 nM human β-catenin was incubated with 5 nM of *C*-terminally fluorescein-labeled human E-cadherin in the assay buffer for 30 min at 4 °C. Different concentrations of the tested compounds in the assay buffer were added to each test plates to make a final volume of 100 μL. For the β-catenin/APC-R3 inhibition assay, 1440 nM human β-catenin was incubated with 5 nM of *C*-terminally fluorescein-labeled human APC-R3 in the assay buffer for 30 min at 4 °C. Different concentrations of the tested compounds in the assay buffer were added to each test plate to make a final volume of 100 μL. In the AlphaScreen competitive inhibition assay for the β-catenin/Tcf4 PPI, 5 nM of *C*-terminally biotinylated human Tcf4 and 20 nM of *N*-terminally His_6-tagged human β-catenin were incubated in an assay buffer of 20 mM HEPES (pH 7.4), 100 mM NaCl, 0.1% BSA, and 0.001% Triton X-100 at 4 °C for 15 min. Different concentrations of the tested compounds (10−12 compound concentrations typically for each compound) were added in 20 μL of assay buffer. The assay plates were covered black and gently mixed on an orbital shaker at 4 °C for 45 min. The streptavidin-coated donor beads and the nickel chelate acceptor beads were added to a final concentration of 10 μg/mL in 25 μL assay buffer. The mixture was incubated for 2 h at 4 °C before detection. The IC_{50} value was then determined by nonlinear least-squares analysis of GraphPad Prism 5.0, and the K_i values were derived.[86]

Compounds Sources. Compounds **15**−**17** and **22**−**25** were purchased from Sigma-Aldrich. Compounds **18** and **21** were purchased from Zelinsky Institute, Inc. (Newark, Delaware, USA) with the catalogue numbers of UZI/7116003 and UZI/2587998. Compound **19** was purchased from InterBioScreen (Moscow, Russia) with the catalogue number of STOCK1S-52622. Compounds **1** and **2** were purchased from Santa Cruz Biotechnology (Santa Cruz, California, USA) with the catalogue numbers of SC-3545 and SC-255013. Compound **3** was purchased from Calbiochem (Billerica, Massachusetts, USA) with the catalogue number of 219331. Compounds **8** and **9** were resynthesized in our lab.

MTs Cell Viability Assay. Colorectal cancer cell lines, SW480, HT29, an HCT116, and human normal cell line HEK293 were seeded in 96-well plates at 4×10^3 cells/well, maintained overnight at 37 °C and incubated with the tested compounds at various concentrations. Cell viability was monitored after 72 h using a freshly prepared mixture of 1 part phenazine methosulfate (PMS, Sigma) solution (0.92 mg/mL) and 19 parts 3-(4,5-dimethylthiazol-2-yl)-5-(3-carboxymethoxyphenyl)-2-(4-sulfophenyl)-2*H*-tetrazolium (MTs, Promega) solution (2 mg/mL). Cells were incubated in 10 μL of this solution at 37 °C for 3 h, and A_{490} was measured. The effect of each compound is expressed as the concentration required to reduce A_{490} by 50% (IC_{50}) relative to DMSO-treated cells. Experiments were performed in triplicate.

Cell Transfection and Luciferase Assay. FuGENE 6 (E2962, Promega) in a 96-well plate format was used for the transfection of HEK293 and SW480 cells according to the manufacturer's instructions. HEK293 cells were cotransfected with 45 ng of the TOPFlash or FOPFlash reporter gene, 135 ng of pcDNA3.1−β-catenin and 20 ng of pCMV-RL normalization reporter gene. SW480 cells were cotransfected with 60 ng of the TOPFlash or FOPFlash reporter gene and 40 ng of pCMV-RL normalization reporter. Cells were cultured in DMEM and 10% fatal bovine serum at 37 °C for 24 h, and different concentrations of inhibitors were then added. After 24 h, the luciferase reporter activity was measured using the Dual-Glo system (E2940, Promega). Normalized luciferase activity in response to the treatment with the inhibitors was compared with that obtained from the cells treated with DMSO. Experiments were performed in triplicate.

Quantitative Real Time PCR Analysis. SW480 cells at 1×10^6/mL were treated with different concentrations of the tested compounds for 24 h. Total RNAs were extracted with TRIzol (15596026, Life Technologies), and the cDNA was synthesized with the superscript III first-strand kit (18080−051, Invitrogen). Quantitative real-time PCR was performed using the iQ SYBR green supermix kit (170−8880, BIO-RAD) on an iQ^5 multicolor real-time PCR reaction system (BIO-RAD). The threshold cycle (C_T) values were normalized to that of internal reference *GAPDH*. The primer pairs for human *GAPDH* were forward, 5′-GAAGGTGAAGGTCGGAGTC-3′, and reverse, 5′-GAAGATGGTGATGGGATTTC-3′; for human *HPRT*, forward, 5′-GCTATAAATTCTTTGCTGACCTGCTG-3′, and reverse, 5′-AATTACTTTTATGTCCCCTGTTGACTGG-3′; for human *AXIN2*, forward, 5′-AGTGTGAGGTCCACGGAAAC-3′, and reverse, 5′-CTTCACACTGCGATGCATTT-3′; for human *c-myc*, forward, 5′-CTTCTCTCCGTCCTCGGATTCT-3′, and reverse, 5′-GAAGGTGATCCAGACTCTGACCTT-3′; and for human *cyclin D1*, forward, 5′-ACAAACAGATCATCCGCAAACAC-3′, and reverse, 5′-TGTTGGGGCTCCTCAGGTTC-3′. Experiments were performed in triplicate.

Western Blotting. SW480 cells at 1×10^6 cells/mL were treated with different concentrations of **18** for 24 h. Cell were lysed in a buffer containing 50 mM Tris (pH 7.4), 150 mM NaCl, 1% Nonidet P-40, 0.5% sodium deoxycholate, 0.1% SDS, and protease inhibitors. After centrifugation at 12000 rpm for 20 min at 4 °C, the supernatant was loaded onto an 8% SDS polyacrylamide gel for electrophoretic analysis. Separated proteins were transferred onto nitrocellulose membranes for immunoblot analysis. The antibodies against c-myc (D84C12, Cell Signaling), cyclin D1 (sc-853, Santa Cruz Biotechnology, Inc.), and β-tubulin (sc-55529, Santa Cruz Biotechnology, Inc.) were used. IRDye 680LT goat antimouse IgG (827−11080, LiCOR) or IRDye 800CW goat antirabbit IgG (827−08365, LiCOR) was used as the secondary antibody. The images were detected by the Odyssey infrared imaging system (LiCOR). The Western blot bands were

DOI: 10.1021/acs.jmedchem.5b00223
J. Med. Chem. XXXX, XXX, XXX−XXX

quantified by LI-COR Image Studio Lite 4.0. Experiments were performed in duplicate.

Coimmunoprecipitation Assay. SW480 cells at 1 × 10^6/mL were treated with different concentrations of **18** for 24 h. Cells were lysed in buffer containing 50 mM Tris, pH 7.4, 150 mM NaCl, 1% Nonidet P-40, 2 mM EDTA, and protease inhibitors. The lysates were preadsorbed to A/G plus agarose (sc-2003, Santa Cruz Biotechnology, Inc.) at 4 °C for 1 h. Preadsorbed lysates were incubated with a specific primary antibody overnight at 4 °C. A/G plus agarose was then added to the lysates mixture and incubated for 3 h. The beads were washed 5 times with the lysis buffer at 4 °C. The bound protein was eluted by boiling in the SDS sample buffer and loaded onto 8% SDS polyacrylamide gel for electrophoretic analysis. Separated proteins were transferred onto nitrocellulose membranes for immunoblot analysis. The primary antibodies were against β-catenin (610153, BD Biosciences) and Tcf4 (05−511, Millipore). IRDye 680LT goat antimouse IgG (827-11080, LiCOR) was used as the secondary antibody. The images were detected by the Odyssey infrared imaging system (LiCOR). Experiments were performed in duplicate.

Ligand Docking using AutoDock Vina. Autodock Vina was used for the initial blind docking of **18**. Exhaustiveness was increased to 12 (exhaustiveness = 1 2), and 18 ligand conformations (num_modes =18) were generated for each binding region. All other parameters were left as default values.

Ligand Docking using Glide 5.8. The 3-D coordinates of all ligands were generated by Schrodinger LigPrep with Epik to expand the protonation and tautomeric states at pH = 7.0. The energy minimization was then applied to all ligands with the OPLS_2005 force field and the GB/SA water solvation condition. The partial charges of the ligands were calculated with the OPLS_2005 force field. The grid box was defined to include all the residues in the Tcf4 $G^{13}ANDE^{17}$ binding site.[57] The default parameters were used in receptor grid generation. The standard precision mode was used in ligand docking. The ligand scaling factor was set to 0.5 for the atoms with the partial charges lower than 0.15. The number of poses per ligand for the initial phase of docking was increased to 10000. The 1000 best poses per ligand were kept for energy minimization with a maximum number of the minimization steps of 5000. A maximum of 100000 ligand poses per docking run and 50 poses per ligand were collected. Up to 100 poses per ligand were kept for the postdocking minimization. The default settings were used for the remaining parameters.

Ligand Docking using AutoDock 4.2. The partial atomic charges were calculated using the Gasteiger−Marsili method. The rotatable bonds in the ligands were defined using AutoTors, which also united the nonpolar hydrogens and partial atomic charges to the bonded carbon atoms. The grid maps were calculated using AutoGrid. The AutoDock area was defined to include all the residues of the Tcf4 $G^{13}ANDE^{17}$ binding site, and the grid spacing was set to 0.375 Å. Docking was performed using the Lamarckian genetic algorithm, and the pseudo-Solis and Wets method was applied for the local search. Each docking experiment was performed 100 times, yielding 100 docked conformations. The other settings were the default parameters. All of the ligands followed the same docking protocol. The results of the docking experiments were evaluated by the auxiliary clustering analysis and the visual inspection.

Chemical Synthesis. *General Methods, Reagents, and Materials.* All reagents were purchased from Aldrich and Acros Organics and used without further purification unless stated otherwise. ^{1}H NMR and ^{13}C NMR spectra were recorded on a Varian VXR-500 (500 MHz), a Varian Inova-400 (400 MHz), or a Varian Unity-300 (300 MHz) spectrometer (125.7, 100, and 75 MHz for ^{13}C NMR spectra, respectively) in DMSO-d_6, acetone-d_6, and $CDCl_3$. Chemical shifts were reported as values in parts per million (ppm), and the reference resonance peaks were set at 7.26 ppm ($CHCl_3$), 2.50 ppm [$(CD_2H)_2SO$], 2.05 ppm [$(CD_2H)_2CO$] for the ^{1}H NMR spectra and 77.23 ppm ($CDCl_3$), 39.52 ppm (DMSO-d_6), and 29.84 ppm (acetone-d_6) for the ^{13}C NMR spectra. Low-resolution and high-resolution mass spectra were determined on a Micromass Quattro II mass spectrometer with an ESI source. Thin-layer chromatography was carried out on E. Merck precoated silica gel 60 F254 plates with visualization accomplished with phosphomolybdic acid or ninhydrin spray reagent or with a UV−visible lamp. Column chromatography was performed with SiliaFlash F60 (230−400 mesh).

*9H-Indeno[1,2-b][1,2,5]oxadiazolo[3,4-e]pyrazin-9-one (**19**).* To a solution of ninhydrin (0.32 g, 1.80 mmol) in a solvent mixture (ethanol:glacial acid = 1:1, 10 mL) was added 1,2,5-oxadiazole-3,4-diamine (0.18 g, 1.80 mmol). After stirring for 18 h at room temperature, the mixture was heated to gentle reflux for another 6 h. It was then cooled to room temperature, and the resulting precipitate was filtered and washed with water to yield **19** as pale-yellow solid (0.29 g, 72% yield). ^{1}H NMR (300 MHz, DMSO-d_6) δ ppm 8.31 (d, J = 7.2 Hz, 1H), 8.18−8.02 (m, 2H), 7.97 (d, J = 7.2 Hz, 1H). ^{13}C NMR (125 MHz, DMSO-d_6) δ ppm 189.55, 161.70, 140.01, 139.95, 138.69, 136.52, 126.06. HRMS (ESI) calcd for $C_{11}H_4N_4O_2$ $(M + Na)^+$ 247.0232, found 247.0230.

*(Z)-9-Hydrazono-9H-indeno[1,2-b][1,2,5]oxadiazolo[3,4-e]pyrazine (**20**).* To a solution of **19** (0.15 g, 0.67 mmol) in a mixture of ethanol and glacial acid (10 mL, 1:1) was added hydrazine hydrate (0.33 g, 6.70 mmol). The mixture was heated to gentle reflux for 2 h and then cooled to room temperature. The resulting precipitate was filtered and washed with water to afford **20** as red solid (0.14 g, 93% yield). ^{1}H NMR (300 MHz, DMSO-d_6) δ ppm 10.48 (d, J = 13.8 Hz, 1H), 10.40 (d, J = 13.8 Hz, 1H), 8.07 (d, J = 7.5 Hz, 1H), 7.73−7.66 (m, 2H), 7.46 (t, J = 7.5 Hz, 1H). ^{13}C NMR (75 MHz, DMSO-d_6) δ ppm 161.75, 155.02, 152.69, 152.51, 144.75, 135.86, 129.81, 128.86, 128.48, 124.66, 119.65. HRMS (ESI) calcd for $C_{11}H_6N_6O$ $(M - H)^-$ 237.0525, found 237.0531.

*4-Amino-1,2,5-oxadiazole-3-carbohydrazide (**40**).* To a solution of 4-amino-1,2,5-oxadiazole-3-carboxylic acid (0.50 g, 3.87 mmol) in methanol (30 mL) was bubbled HCl (gas). The mixture was heated to gentle reflux for 8 h. Methanol was then removed under vacuum to give the crude product as pale-yellow oil. To this residue was added diethyl ether (30 mL) and stirred for 30 min. The resulting precipitate was filtered to give desired product **39** (0.50 g, 91% yield) as white solid. It was used directly in next step without further purification. To a solution of **39** (0.15 g, 1.05 mmol) in methanol (10 mL) was added hydrazine hydrate (0.08 g, 1.57 mmol), and the mixture was heated to gentle reflux. After 15 h, the solvent was removed completely under vacuum to give **40** (0.09 g, 60% yield) as white solid. ^{1}H NMR (500 MHz, acetone-d_6) δ ppm 9.50 (brs, 1H), 5.76 (s, 2H), 4.50 (brs, 2H). ^{13}C NMR (-d_6) δ ppm 157.02, 156.06, 140.00. HRMS (ESI) calcd for $C_3H_5N_5O_2$ $(M + H)^+$ 144.0516, found 144.0519.

*(Z)-4-Amino-N′-(9H-indeno[1,2-b][1,2,5]oxadiazolo[3,4-e]pyrazin-9-ylidene)-1,2,5-oxadiazole-3-carbohydrazide (**18**).* To a solution of **19** (0.05 g, 0.22 mmol) in ethanol (10 mL) was added **40** (0.03 g, 0.22 mmol) and glacial acid (1 mL). The reaction mixture was heated to gentle reflux overnight and then poured into ice water. The resulting precipitate was filtered and washed with water to give **18** as yellow solid (0.06 g, 78% yield). ^{1}H NMR (500 MHz, DMSO-d_6) δ ppm 13.55 (brs, 1H), 8.26 (d, J = 7.5 Hz, 1H), 8.06 (d, J = 7.0 Hz, 1H), 7.92 (t, J = 7.5 Hz, 1H), 7.82 (t, J = 7.0 Hz, 1H), 6.01 (s, 2H). ^{13}C NMR (125 MHz, DMSO-d_6) δ ppm 162.75, 158.62, 157.14, 155.38, 153.17, 152.29, 152.04, 144.32, 140.35, 136.76, 134.59, 133.67, 125.23, 122.82. HRMS (ESI) calcd for $C_{14}H_7N_9O_3$ $(M - H)^-$ 348.0594, found 348.0604.

*5H-[1,2,5]Oxadiazolo[3′,4′:5,6]pyrazino[2,3-b]indole (**27**).* To a solution of isatin (0.20 g, 1.36 mmol) in glacial acid (5 mL) was added 1,2,5-oxadiazole-3,4-diamine (0.14 g, 1.36 mmol). The resulting mixture was heated to gentle reflux for 15 h and then poured into ice water. The resulting precipitate was filtered and washed with water to afford **27** as red solid (0.05 g, 17% yield). ^{1}H NMR (300 MHz, DMSO-d_6) δ ppm 12.35 (brs, 1H), 8.19 (d, J = 7.8 Hz, 1H), 7.73 (t, J = 7.5 Hz, 1H), 7.39 (d, J = 8.1 Hz, 1H), 7.32 (t, J = 7.2 Hz, 1H). ^{13}C NMR (75 MHz, DMSO-d_6) δ ppm 153.96, 152.62, 152.50, 151.93, 148.81, 136.37, 125.33, 123.11, 118.86, 113.38. HRMS (ESI) calcd for $C_{10}H_5N_5O$ $(M - H)^-$ 210.0416, found 210.0427.

*Ethyl-2-(5H-[1,2,5]oxadiazolo[3′,4′:5,6]pyrazino[2,3-b]indol-5-yl)acetate (**28**).* To a solution of **27** (0.08 g, 0.38 mmol) and ethyl 2-

DOI: 10.1021/acs.jmedchem.5b00223
J. Med. Chem. XXXX, XXX, XXX−XXX

bromoacetate (0.09 g, 0.57 mmol) in DMSO (10 mL) was added K_2CO_3 (0.08 g, 0.57 mmol). The resulting mixture was heated to 80 °C overnight. After 15 h, the reaction mixture was cooled to room temperature and diluted with ethyl acetate (80 mL), washed with brine (20 mL × 3), dried over Na_2SO_4, filtered, and concentrated. The residue was purified by column chromatography (silica gel, hexanes:acetone = 5:1) to afford **28** (0.08 g, 73% yield) as red solid. ^{1}H NMR (500 MHz, DMSO-d_6) δ ppm 8.28 (d, J = 7.5 Hz, 1H), 7.85 (t, J = 7.0 Hz, 1H), 7.69 (d, J = 8.5 Hz, 1H), 7.42 (t, J = 7.5 Hz, 1H), 5.22 (s 2H), 4.18 (q, J = 7.0 Hz, 2H), 1.21 (t, J = 7.0 Hz, 3H). ^{13}C NMR (125 MHz, DMSO-d_6) δ ppm 167.98, 153.15, 152.32, 152.07, 151.64, 148.92, 136.50, 125.30, 124.05, 118.50, 112.39, 62.25, 43.35, 14.70. HRMS (ESI) calcd for $C_{14}H_{11}N_5O_3$ $(M + Na)^+$ 320.0760, found 320.0759.

*2-(5H-[1,2,5]Oxadiazolo[3′,4′:5,6]pyrazino[2,3-b]indol-5-yl)acetic Acid (**29**).* To a solution of **28** (0.08 g, 0.27 mmol) in a solvent mixture (14 mL, THF:MeOH:H_2O = 4:2:1) was added LiOH (0.05 g, 2.15 mmol). The mixture was stirred for 8 h at room temperature. Then, the pH value was adjusted to 4−5 with HCl (1 M), diluted with water (50 mL), and extracted with ethyl acetate (20 mL × 3). The combined organic phase was dried over Na_2SO_4 and concentrated to give **29** (0.05g, 68%) as orange solid. ^{1}H NMR (500 MHz, DMSO-d_6) δ ppm 13.36 (brs, 1H), 8.28 (d, J = 8.0 Hz, 1H), 7.84 (t, J = 8.0 Hz, 1H), 7.69 (d, J = 8.0 Hz, 1H), 7.41 (t, J = 8.0 Hz, 1H), 5.10 (s, 2H). ^{13}C NMR (125 MHz, DMSO-d_6) δ ppm 169.34, 153.20, 153.00, 152.11, 151.63, 149.10, 136.51, 125.27, 123.95, 118.44, 112.38, 43.38. HRMS (ESI) calcd for $C_{12}H_7N_5O_3$ $(M - H)^-$ 268.0471, found 268.0485.

*2-(5H-[1,2,5]Oxadiazolo[3′,4′:5,6]pyrazino[2,3-b]indol-5-yl)-N-(4-amino-1,2,5-oxadiazol-3-yl)acetamide (**26**).* To a solution of **29** (0.18 g, 0.67 mmol) and 4-methylmorpholine (0.14 g, 0.34 mmol) in THF (15 mL) was added isobutyl chloroformate (0.09 g, 0.67 mmol) at −15 °C. The resulting mixture was stirred for 1 h at the same temperature. Then 1,2,5-oxadiazole-3,4-diamine (0.10 g, 1.00 mmol) was added slowly. The temperature was allowed to rise to room temperature gradually and stirred for another 1 h. The mixture was diluted with ethyl acetate (80 mL), washed with brine (20 mL × 3), dried over Na_2SO_4, filtrated, and concentrated. The residue was purified by column chromatography (silica gel, hexanes:acetone = 2:1 to 1:1) to afford **26** (0.12 g, 51% yield) as orange solid. ^{1}H NMR (500 MHz, DMSO-d_6) δ ppm 11.13 (brs, 1H), 8.32 (d, J = 7.5 Hz, 1H), 7.87 (t, J = 8.0 Hz, 1H), 7.73 (d, J = 8.0 Hz, 1H), 7.45 (t, J = 7.5 Hz, 1H), 6.04 (s, 2H), 5.29 (s, 2H). ^{13}C NMR (125 MHz, DMSO-d_6) δ ppm 166.66, 153.50, 152.88, 152.36, 152.13, 151.96, 149.26, 144.25, 136.50, 125.26, 124.04, 118.69, 112.57, 44.85. HRMS (ESI) calcd for $C_{14}H_9N_9O_3$ $(M - H)^-$ 350.0750, found 350.0755.

*Ethyl 4-(5H-[1,2,5]Oxadiazolo[3′,4′:5,6]pyrazino[2,3-b]indol-5-yl)butanoate (**32**).* To a solution of **27** (0.017 g, 0.08 mmol) in DMF (5 mL) was added NaH (0.0030 g, 0.12 mmol) at 0 °C. The resulting mixture was stirred for 0.5 h at 0 °C before adding ethyl 4-bromobutanoate (0.023 g, 0.12 mmol). The reaction solution was allowed to warm to room temperature gradually then stirred overnight. The mixture was diluted with ethyl acetate (50 mL), washed with brine (20 mL × 3), dried over Na_2SO_4, filtrated, and concentrated. The residue was purified through column chromatography (silica gel, hexanes:acetone = 3:1 to 1:1) to afford **32** as orange solid (0.010 g, yield 58%). ^{1}H NMR (400 MHz, $CDCl_3$) δ ppm 8.20 (d, J = 7.2 Hz, 1H), 7.71 (t, J = 7.2 Hz, 1H), 7.42 (d, J = 8.0 Hz, 1H), 7.31 (t, J = 7.2 Hz, 1H), 4.32 (t, J = 6.8 Hz, 2H), 4.07 (q, J = 6.0 Hz, 2H), 2.43 (t, J = 6.4 Hz, 2H), 2.20−2.12 (m, 2H) 1.19 (t, J = 6.0 Hz, 3H). ^{13}C NMR (100 MHz, $CDCl_3$) δ ppm 172.54, 151.80, 151.27, 151.19, 150.41, 147.98, 135.56, 125.06, 123.11, 118.23, 110.64, 60.71, 40.93, 30.94, 22.68, 14.12. HRMS (ESI) calcd for $C_{16}H_{15}N_5O_3$ $(M + Na)^+$ 348.1073, found 348.1081.

*Methyl 3-(5H-[1,2,5]Oxadiazolo[3′,4′:5,6]pyrazino[2,3-b]indol-5-yl)propanoate (**30**).* To a solution of **27** (0.10 g, 0.47 mmol) in acetonitrile (15 mL) was added 1,8-diazabicyclo[5.4.0]undec-7-ene (DBU) (0.24 g, 1.57 mmol). The resulting mixture was stirred for 0.5 h before adding methyl acrylate (0.14 g, 1.57 mmol). The reaction solution was heated to 50 °C and stirred for another 24 h. It was then diluted with ethyl acetate (50 mL), washed with brine (20 mL × 3), and dried over Na_2SO_4, filtrated, and concentrated. The residue was purified by column chromatography (silica gel, hexanes:acetone = 3:1 to 1:1) to afford **30** as orange solid (0.084 g, yield 60%). ^{1}H NMR (400 MHz, $CDCl_3$) δ ppm 8.33 (d, J = 7.6 Hz, 1H), 7.79 (t, J = 8.4 Hz, 1H), 7.51 (d, J = 8.4 Hz, 1H), 7.40 (t, J = 7.6 Hz, 1H), 4.60 (t, J = 6.8 Hz, 2H), 3.66 (s, 3H), 3.02 (t, J = 6.8 Hz, 2H). ^{13}C NMR (100 MHz, $CDCl_3$) δ ppm 171.27, 151.81, 151.39, 151.16, 150.42, 147.90, 135.48, 125.20, 123.25, 118.42, 110.81, 52.11, 37.90, 21.11. HRMS (ESI) calcd for $C_{14}H_{11}N_5O_3$ $(M + Na)^+$ 320.0760, found 320.0760.

*3-(5H-[1,2,5]Oxadiazolo[3′,4′:5,6]pyrazino[2,3-b]indol-5-yl)-propanoic Acid (**31**).* Orange solid, and yield 80%. ^{1}H NMR (400 MHz, DMSO-d_6) δ ppm 12.46 (brs, 1H), 8.26 (d, J = 7.6 Hz, 1H), 7.85 (t, J = 8.0 Hz, 1H), 7.76 (d, J = 8.0 Hz, 1H), 7.40 (t, J = 7.6 Hz, 1H), 4.48 (t, J = 6.8 Hz, 2H), 2.83 (t, J = 7.2 Hz, 2H). ^{13}C NMR (100 MHz, DMSO-d_6) δ ppm 172.65, 153.56, 152.09, 151.96, 151.49, 148.66, 136.88, 124.99, 123.33, 118.52, 112.25, 32.10, 31.14. HRMS (ESI) calcd for $C_{13}H_9N_5O_3$ $(M + Na)^+$ 306.0603, found 306.0612.

*4-(5H-[1,2,5]Oxadiazolo[3′,4′:5,6]pyrazino[2,3-b]indol-5-yl)-butanoic Acid (**33**).* Orange solid, and yield 65%. ^{1}H NMR (400 MHz, DMSO-d_6) δ ppm 12.08 (brs, 1H), 8.27 (d, J = 7.6 Hz, 1H), 7.86 (t, J = 8.0 Hz, 1H), 7.70 (d, J = 8.0 Hz, 1H), 7.41 (t, J = 7.2 Hz, 1H), 4.30 (t, J = 6.8 Hz, 2H), 2.38 (t, J = 7.2 Hz, 2H), 2.07−2.00 (m, 2H). ^{13}C NMR (100 MHz, DMSO-d_6) δ ppm 174.38, 153.67, 152.21, 151.97, 148.78, 136.10, 125.11, 123.29, 118.60, 111.76, 109.99, 41.07, 31.23, 23.06. HRMS (ESI) calcd for $C_{14}H_{11}N_5O_3$ $(M + Na)^+$ 320.0760, found 320.0761.

*2-(5H-[1,2,5]Oxadiazolo[3′,4′:5,6]pyrazino[2,3-b]indol-5-yl)-acetonitrile (**34**).* To a solution of **27** (0.03 g, 0.14 mmol) in DMF (10 mL) was added NaH (60%) (0.007 g, 0.17 mmol) at 0 °C. The resulting mixture was stirred for 0.5 h at the same temperature before 2-bromoacetonitrile (0.02 g, 0.17 mmol) was added into it. It was then allowed to warm to room temperature gradually and stirred for another 1 h. The reaction mixture was then quenched with water (30 mL) and diluted with ethyl acetate (60 mL). The organic phase was washed with brine (20 mL × 2), dried over Na_2SO_4, and concentrated. The residue was purified by column chromatography (silica gel, hexanes:acetone = 5:1) to afford **34** (0.025 g, 71% yield) as yellow solid. ^{1}H NMR (500 MHz, acetone-d_6) δ ppm 8.37 (d, J = 8.0 Hz, 1H), 7.97 (t, J = 8.5 Hz, 1H), 7.85 (d, J = 8.5 Hz, 1H), 7.56 (t, J = 8.0 Hz, 1H), 5.51 (s 2H). ^{13}C NMR (125 MHz, acetone-d_6) δ ppm 152.75, 152.33, 151.73, 151.12, 147.17, 135.97, 125.04, 124.21, 119.23, 114.31, 111.31, 29.44. HRMS (ESI) calcd for $C_{12}H_6N_6O$ $(M + Na)^+$ 273.0501, found 273.0508.

*4-(5H-[1,2,5]Oxadiazolo[3′,4′:5,6]pyrazino[2,3-b]indol-5-yl)-butanenitrile (**36**).* Orange solid, yield 50%. ^{1}H NMR (400 MHz, DMSO-d_6) δ ppm 7.61−7.64 (m, 2H), 7.16 (t, J = 7.6 Hz, 1H), 6.97 (d, J = 8.0 Hz, 1H), 3.87 (t, J = 7.2 Hz, 2H), 2.48 (t, J = 7.2 Hz, 2H), 2.11−2.07 (m, 2H). ^{13}C NMR (100 MHz, DMSO-d_6) δ ppm 158.41, 150.19, 138.62, 125.81, 124.16, 118.61, 117.73, 109.77, 38.85, 23.49, 15.02. HRMS (ESI) calcd for $C_{14}H_{10}N_6O$ $(M + Na)^+$ 301.0814, found 301.0808.

*3-(5H-[1,2,5]Oxadiazolo[3′,4′:5,6]pyrazino[2,3-b]indol-5-yl)-propanenitrile (**35**).* To a solution of **27** (0.20 g, 0.95 mmol) in acetonitrile (10 mL), DBU (0.072 g, 0.47 mmol) was added. The solution was stirred for 0.5 h. Then, acrylonitrile (0.075 g, 1.4 mmol) was added. The reaction solution was heated to 50 °C and stirred for 24 h. It was then diluted with ethyl acetate (50 mL), washed with brine (20 mL × 3), and dried over Na_2SO_4, filtrated, and concentrated. The residue was purified by column chromatography (silica gel, hexanes:acetone = 5:1 to 1:1) to afford **35** as orange solid (yield 62%). ^{1}H NMR (400 MHz, DMSO-d_6) δ ppm 8.28 (d, J = 7.6 Hz, 1H), 7.89−7.84 (m, 2H), 7.42 (t, J = 7.2 Hz, 1H), 4.61 (t, J = 6.8 Hz, 2H), 3.10 (t, J = 6.4 Hz, 2H). ^{13}C NMR (100 MHz, DMSO-d_6) δ ppm 153.39, 152.02, 151.94, 151.51, 148.27, 136.17, 125.11, 123.69, 119.10, 118.51, 112.17, 37.66, 16.43. HRMS (ESI) calcd for $C_{13}H_8N_6O$ $(M + Na)^+$ 287.0657, found 287.0661.

*5-(2-(2H-Tetrazol-5-yl)ethyl)-5H-[1,2,5]oxadiazolo[3′,4′:5,6]-pyrazino[2,3-b]indole (**37**).* To a solution of **35** (0.02 g, 0.076 mmol) in toluene (10 mL) was added nBu$_3$SnN$_3$ (0.13 g, 0.38 mmol). The resulting mixture was heated to reflux for 48 h. It was then cooled to

DOI: 10.1021/acs.jmedchem.5b00223
J. Med. Chem. XXXX, XXX, XXX−XXX

room temperature, and the pH value was adjusted to 4−5 with HCl (1 M) and diluted with ethyl acetate (60 mL). The organic phase was washed with brine (20 mL × 2), dried over Na_2SO_4, and concentrated. The residue was purified by column chromatography (silica gel, CH_2Cl_2:MeOH = 10:1 to 5:1) to afford **37** (15.00 mg, 65% yield) as red solid. ^{1}H NMR (500 MHz, DMSO-d_6) δ ppm 8.28 (d, J = 7.8 Hz, 1H), 7.81 (t, J = 8.1 Hz, 1H), 7.58 (d, J = 8.0 Hz, 1H), 7.39 (t, J = 7.8 Hz, 1H), 4.66 (t, J = 6.6 Hz, 2H), 3.46 (t, J = 6.6 Hz, 2H). ^{13}C NMR (125 MHz, DMSO-d_6) δ ppm 154.29, 153.81, 152.22, 152.17, 151.79, 148.66, 136.36, 125.33, 123.69, 118.74, 111.92, 40.36, 22.30. HRMS (ESI) calcd for $C_{13}H_9N_9O$ $(M - H)^-$ 306.0852, found 306.0871.

*5-(3-(2H-Tetrazol-5-yl)propyl)-5H-[1,2,5]oxadiazolo[3′,4′:5,6]-pyrazino[2,3-b]indole (**38**).* Red solid, yield 57%. ^{1}H NMR (500 MHz, DMSO-d_6) δ ppm 8.26 (d, J = 8.0 Hz, 1H), 7.85 (t, J = 8.0 Hz, 1H), 7.72 (d, J = 8.5 Hz, 1H), 7.40 (t, J = 7.5 Hz, 1H), 4.40 (t, J = 6.5 Hz, 2H), 3.02 (t, J = 7.5 Hz, 2H), 2.32−2.26 (m, 2H). ^{13}C NMR (125 MHz, DMSO-d_6) δ ppm 153.81, 152.35, 152.18, 151.91, 148.92, 136.35, 125.32, 123.58, 118.82, 112.06, 41.32, 25.55, 21.10. HRMS (ESI) calcd for $C_{14}H_{11}N_9O$ $(M + Na)^+$ 344.0984, found 344.0990.

■ ASSOCIATED CONTENT

Ⓢ Supporting Information

Assay results, HPLC conditions, and HPLC tracers (PDF, CSV). The Supporting Information is available free of charge on the ACS Publications website at DOI: 10.1021/acs.jmedchem.5b00223.

■ AUTHOR INFORMATION

Corresponding Author

*Phone: (801) 581-6747. Fax: (801) 581-8433. E-mail: markji@chem.utah.edu.

Author Contributions

†J.L.C. and Y.Z. contributed equally to this work.

Notes

The authors declare no competing financial interest.

■ ACKNOWLEDGMENTS

This work was in part supported by the Pulmonary Fibrosis Foundation I. M. Rosenzweig Young Investigator Award (award number 235170). We thank David A. Jones at the Univeristy of Utha for the TOPFlash, FOPFlash, and β-catenin expression constructs and the Center for High-Performance Computing at the University of Utah for computer time.

■ ABBREVIATIONS USED

APC, adenomatous polyposis coli; DCC, dynamic combinatorial chemistry; FP, fluorescence polarization; K_d, dissociation constant; LC/MS, liquid chromatography/mass spectrometry; PPI, protein−protein interaction; PAINS, pan assay interference compounds; Tcf, T-cell factor

■ REFERENCES

(1) Cousins, G. R. L.; Poulsen, S.-A.; Sanders, J. K. M. Dynamic combinatorial libraries of pseudo-peptide hydrazone macrocycles. *Chem. Commun.* **1999**, 1575−1576.

(2) Poulsen, S.-A. Direct screening of a dynamic combinatorial library using mass spectrometry. *J. Am. Soc. Mass Spectrom.* **2006**, *17*, 1074−1080.

(3) Bhat, V. T.; Caniard, A. M.; Luksch, T.; Brenk, R.; Campopiano, D. J.; Greaney, M. F. Nucleophilic catalysis of acylhydrazone equilibration for protein-directed dynamic covalent chemistry. *Nature Chem.* **2010**, *2*, 490−497.

(4) Bunyapaiboonsri, T.; Ramström, O.; Lohmann, S.; Lehn, J.-M.; Peng, L.; Goeldner, M. Dynamic deconvolution of a pre-equilibrated dynamic combinatorial library of acetylcholinesterase inhibitors. *ChemBioChem* **2001**, *2*, 438−444.

(5) Bunyapaiboonsri, T.; Ramström, H.; Ramström, O.; Haiech, J.; Lehn, J.-M. Generation of bis-cationic heterocyclic inhibitors of *Bacillus subtilis* HPr kinase/phosphatase from a ditopic dynamic combinatorial library. *J. Med. Chem.* **2003**, *46*, 5803−5811.

(6) Mondal, M.; Radeva, N.; Köster, H.; Park, A.; Potamitis, C.; Zervou, M.; Klebe, G.; Hirsch, A. K. H. Structure-based design of inhibitors of the aspartic protease endothiapepsin by exploiting dynamic combinatorial chemistry. *Angew. Chem., Int. Ed.* **2014**, *53*, 3259−3263.

(7) Jiang, Q.-Q.; Sicking, W.; Ehlers, M.; Schmuck, C. Discovery of potent inhibitors of human β-tryptase from pre-equilibrated dynamic combinatorial libraries. *Chem. Sci.* **2015**, *6*, 1792−1800.

(8) Wang, L.; Zuercher, W. J.; Consler, T. G.; Lambert, M. H.; Miller, A. B.; Orband-Miller, L. A.; McKee, D. D.; Willson, T. M.; Nolte, R. T. X-ray crystal structures of the estrogen-related receptor-γ ligand binding domain in three functional states reveal the molecular basis of small molecule regulation. *J. Biol. Chem.* **2006**, *281*, 37773−37781.

(9) Zhang, L.; Liu, W.; Hu, T.; Du, L.; Luo, C.; Chen, K.; Shen, X.; Jiang, H. Structural basis for catalytic and inhibitory mechanisms of β-hydroxyacyl-acyl carrier protein dehydratase (FabZ). *J. Biol. Chem.* **2008**, *283*, 5370−5379.

(10) He, L.; Zhang, L.; Liu, X.; Li, X.; Zheng, M.; Li, H.; Yu, K.; Chen, K.; Shen, X.; Jiang, H.; Liu, H. Discovering potent inhibitors against the β-hydroxyacyl-acyl carrier protein dehydratase (FabZ) of *Helicobacter pylori*: structure-based design, synthesis, bioassay, and crystal structure determination. *J. Med. Chem.* **2009**, *52*, 2465−2481.

(11) Dai, R.; Wilson, D. J.; Geders, T. W.; Aldrich, C. C.; Finzel, B. C. Inhibition of *Mycobacterium tuberculosis* transaminase BioA by aryl hydrazines and hydrazides. *ChemBioChem* **2014**, *15*, 575−586.

(12) Mondal, M.; Radeva, N.; Köster, H.; Park, A.; Potamitis, C.; Zervou, M.; Klebe, G.; Hirsch, A. K. H. Structure-based design of inhibitors of the aspartic protease endothiapepsin by exploiting dynamic combinatorial chemistry. *Angew. Chem., Int. Ed.* **2014**, *53*, 3259−3263.

(13) Baell, J. B.; Holloway, G. A. New substructure filters for removal of pan assay interference compounds (PAINS) from screening libraries and for their exclusion in bioassays. *J. Med. Chem.* **2010**, *53*, 2719−2740.

(14) Malvezzi, A.; de Rezende, L.; Izidoro, M. A.; Cezari, M. H. S.; Juliano, L.; do Amaral, A. T. Uncovering false positives on a virtual screening search for cruzain inhibitors. *Bioorg. Med. Chem. Lett.* **2008**, *18*, 350−354.

(15) Narang, R.; Narasimhan, B.; Sharma, S. A review on biological activities and chemical synthesis of hydrazide derivatives. *Curr. Med. Chem.* **2012**, *19*, 569−612.

(16) Clevers, H.; Nusse, R. Wnt/β-catenin signaling and disease. *Cell* **2012**, *149*, 1192−1205.

(17) Klaus, A.; Birchmeier, W. Wnt signalling and its impact on development and cancer. *Nature Rev. Cancer* **2008**, *8*, 387−398.

(18) Tetsu, O.; McCormick, F. β-Catenin regulates expression of cyclin D1 in colon carcinoma cells. *Nature* **1999**, *398*, 422−426.

(19) He, T.-C.; Sparks, A. B.; Rago, C.; Hermeking, H.; Zawel, L.; da Costa, L. T.; Morin, P. J.; Vogelstein, B.; Kinzler, K. W. Identification of c-MYC as a target of the APC pathway. *Science* **1998**, *281*, 1509−1512.

(20) Kim, P. J.; Plescia, J.; Clevers, H.; Fearon, E. R.; Altieri, D. C. Survivin and molecular pathogenesis of colorectal cancer. *Lancet* **2003**, *362*, 205−209.

(21) Malanchi, I.; Peinado, H.; Kassen, D.; Hussenet, T.; Metzger, D.; Chambon, P.; Huber, M.; Hohl, D.; Cano, A.; Birchmeier, W.; Huelsken, J. Cutaneous cancer stem cell maintenance is dependent on β-catenin signalling. *Nature* **2008**, *452*, 650−653.

(22) Barker, N.; Ridgway, R. A.; van Es, J. H.; van de Wetering, M.; Begthel, H.; van den Born, M.; Danenberg, E.; Clarke, A. R.; Sansom, O. J.; Clevers, H. Crypt stem cells as the cells-of-origin of intestinal cancer. *Nature* **2009**, *457*, 608−611.

DOI: 10.1021/acs.jmedchem.5b00223
J. Med. Chem. XXXX, XXX, XXX−XXX

(23) Yeung, J.; Esposito, M. T.; Gandillet, A.; Zeisig, B. B.; Griessinger, E.; Bonnet, D.; So, C. W. E. β-Catenin mediates the establishment and drug resistance of MLL leukemic stem cells. *Cancer Cell* **2010**, *18*, 606−618.
(24) Kim, J.-S.; Crooks, H.; Foxworth, A.; Waldman, T. Proof-of-principle: oncogenic β-catenin is a valid molecular target for the development of pharmacological inhibitors. *Mol. Cancer Ther.* **2002**, *1*, 1355−1359.
(25) Ashihara, E.; Kawata, E.; Nakagawa, Y.; Shimazaski, C.; Kuroda, J.; Taniguchi, K.; Uchiyama, H.; Tanaka, R.; Yokota, A.; Takeuchi, M.; Kamitsuji, Y.; Inaba, T.; Taniwaki, M.; Kimura, S.; Maekawa, T. β-Catenin small interfering RNA successfully suppressed progression of multiple myeloma in a mouse model. *Clin. Cancer Res.* **2009**, *15*, 2731−2738.
(26) Scholer-Dahirel, A.; Schlabach, M. R.; Loo, A.; Bagdasarian, L.; Meyer, R.; Guo, R.; Woolfenden, S.; Yu, K. K.; Markovits, J.; Killary, K.; Sonkin, D.; Yao, Y.-M.; Warmuth, M.; Sellers, W. R.; Schlegel, R.; Stegmeier, F.; Mosher, R. E.; McLaughlin, M. E. Maintenance of adenomatous polyposis coli (APC)-mutant colorectal cancer is dependent on Wnt/β-catenin signaling. *Proc. Natl. Acad. Sci. U. S. A.* **2011**, *108*, 17135−17140.
(27) Graham, T. A.; Ferkey, D. M.; Mao, F.; Kimelman, D.; Xu, W. Tcf4 can specifically recognize β-catenin using alternative conformations. *Nature Struct. Biol.* **2001**, *8*, 1048−1052.
(28) Poy, F.; Lepourcelet, M.; Shivdasani, R. A.; Eck, M. J. Structure of a human Tcf4−β-catenin complex. *Nature Struct. Biol.* **2001**, *8*, 1053−1057.
(29) Sampietro, J.; Dahlberg, C. L.; Cho, U. S.; Hinds, T. R.; Kimelman, D.; Xu, W. Crystal structure of a β-catenin/BCL9/Tcf4 complex. *Mol. Cell* **2006**, *24*, 293−300.
(30) Sun, J.; Weis, W. I. Biochemical and structural characterization of β-catenin interactions with nonphosphorylated and CK2-phosphorylated Lef-1. *J. Mol. Biol.* **2011**, *405*, 519−530.
(31) Graham, T. A.; Weaver, C.; Mao, F.; Kimelman, D.; Xu, W. Crystal structure of a β-catenin/Tcf complex. *Cell* **2000**, *103*, 885−896.
(32) Knapp, S.; Zamai, M.; Volpi, D.; Nardese, V.; Avanzi, N.; Breton, J.; Plyte, S.; Flocco, M.; Marconi, M.; Isacchi, A.; Caiolfa, V. R. Thermodynamics of the high-affinity interaction of TCF4 with β-catenin. *J. Mol. Biol.* **2001**, *306*, 1179−1189.
(33) Yu, B.; Huang, Z.; Zhang, M.; Dillard, D. R.; Ji, H. Rational design of small-molecule inhibitors for β-catenin/T-cell factor protein−protein interactions by bioisostere replacement. *ACS Chem. Biol.* **2013**, *8*, 524−529.
(34) von Kries, J. P.; Winbeck, G.; Asbrand, C.; Schwarz-Romond, T.; Sochnikova, N.; Dell'Oro, A.; Behrens, J.; Birchmeier, W. Hot spots in β-catenin for interactions with LEF-1, conductin and APC. *Nature Struct. Biol.* **2000**, *7*, 800−807.
(35) Gail, R.; Frank, R.; Wittinghofer, A. Systematic peptide array-based delineation of the differential β-catenin interaction with Tcf4, E-cadherin, and adenomatous polyposis coli. *J. Biol. Chem.* **2005**, *280*, 7107−7117.
(36) Xing, Y.; Clements, W. K.; Kimelman, D.; Xu, W. Crystal structure of a β-catenin/axin complex suggests a mechanism for the β-catenin destruction complex. *Genes Dev.* **2003**, *17*, 2753−2764.
(37) Huber, A. H.; Weis, W. I. The structure of the β-catenin/E-cadherin complex and the molecular basis of diverse ligand recognition by β-catenin. *Cell* **2001**, *105*, 391−402.
(38) Spink, K. E.; Fridman, S. G.; Weis, W. I. Molecular mechanisms of β-catenin recognition by adenomatous polyposis coli revealed by the structure of an APC−β-catenin complex. *EMBO J.* **2001**, *20*, 6203−6212.
(39) Ha, N.-C.; Tonozuka, T.; Stamos, J. L.; Choi, H.-J.; Weis, W. I. Mechanism of phosphorylation-dependent binding of APC to β-catenin and its role in β-catenin degradation. *Mol. Cell* **2004**, *15*, 511−521.
(40) Xing, Y.; Clements, W. K.; Le Trong, I.; Hinds, T. R.; Stenkamp, R.; Kimelman, D.; Xu, W. Crystal structure of a β-catenin/APC complex reveals a critical role for APC phosphorylation in APC function. *Mol. Cell* **2004**, *15*, 523−533.
(41) Orsulic, S.; Huber, O.; Aberle, H.; Arnold, S.; Kemler, R. E-cadherin binding prevents β-catenin nuclear localization and β-catenin/LEF-1-mediated transactivation. *J. Cell Sci.* **1999**, *112*, 1237−1245.
(42) Choi, H.-J.; Huber, A. H.; Weis, W. I. Thermodynamics of β-catenin−ligand interactions: the roles of the *N*- and *C*-terminal tails in modulating binding affinity. *J. Biol. Chem.* **2006**, *281*, 1027−1038.
(43) Sun, J.; Weis, W. I. Biochemical and structural characterization of β-catenin interactions with nonphosphorylated and CK2-phosphorylated Lef-1. *J. Mol. Biol.* **2011**, *405*, 519−530.
(44) Choi, H.-J.; Gross, J. C.; Pokutta, S.; Weis, W. I. Interactions of plakoglobin and β-catenin with desmosomal cadherins: basis of selective exclusion of α- and β-catenin from desmosomes. *J. Biol. Chem.* **2009**, *284*, 31776−31788.
(45) Tickenbrock, L.; Köβmeier, K.; Rehmann, H.; Herrmann, C.; Müller, O. Differences between the interaction of β-catenin with non-phosphorylated and single-mimicked phosphorylated 20-amino acid residue repeats of the APC protein. *J. Mol. Biol.* **2003**, *327*, 359−367.
(46) Liu, J.; Xing, Y.; Hinds, T. R.; Zheng, J.; Xu, W. The third 20 amino acid repeat is the tightest binding site of APC for β-catenin. *J. Mol. Biol.* **2006**, *360*, 133−144.
(47) Lepourcelet, M.; Chen, Y.-N. P.; France, D. S.; Wang, H.; Crews, P.; Petersen, F.; Bruseo, C.; Wood, A. W.; Shivdasani, R. A. Small-molecule antagonists of the oncogenic Tcf/β-catenin protein complex. *Cancer Cell* **2004**, *5*, 91−102.
(48) Halbedl, S.; Kratzer, M.-C.; Rahm, K.; Crosta, N.; Masters, K.-S.; Zippert, J.; Bräse, S.; Gradl, D. Synthesis of novel inhibitors blocking Wnt signaling downstream of β-catenin. *FEBS Lett.* **2013**, *587*, 522−527.
(49) Baell, J.; Walters, M. A. Chemistry: chemical con artists foil drug discovery. *Nature* **2014**, *513*, 481−483.
(50) Trosset, J.-Y.; Dalvit, C.; Knapp, S.; Fasolini, M.; Veronesi, M.; Mantegani, S.; Gianellini, L. M.; Catana, C.; Sundström, M.; Stouten, P. F. W.; Moll, J. K. Inhibition of protein−protein interactions: the discovery of druglike β-catenin inhibitors by combining virtual and biophysical screening. *Proteins* **2006**, *64*, 60−67.
(51) Gonsalves, F. C.; Klein, K.; Carson, B. B.; Katz, S.; Ekas, L. A.; Evans, S.; Nagourney, R.; Cardozo, T.; Brown, A. M.; DasGupta, R. An RNAi-based chemical genetic screen identifies three small-molecule inhibitors of the Wnt/wingless signaling pathway. *Proc. Natl. Acad. Sci. U. S. A.* **2011**, *108*, 5954−5963.
(52) Baell, J. B. Observations on screening-based research and some concerning trends in the literature. *Future Med. Chem.* **2010**, *2*, 1529−1546.
(53) Tomašić, T.; Mašič, L. P. Rhodanine as a privileged scaffold in drug discovery. *Curr. Med. Chem.* **2009**, *16*, 1596−1629.
(54) Lee, E.; Mada, A.; David, G.; Garabedian, M. J.; DasGupta, R.; Logan, S. K. Inhibition of androgen receptor and β-catenin activity in prostate cancer. *Proc. Natl. Acad. Sci. U. S. A.* **2013**, *110*, 15710−15715.
(55) Tian, W.; Han, X.; Yan, M.; Xu, Y.; Duggineni, S.; Lin, N.; Luo, G.; Li, Y. M.; Han, X.; Huang, Z.; An, J. Structure-based discovery of a novel inhibitor targeting the β-catenin/Tcf4 interaction. *Biochemistry* **2012**, *51*, 724−731.
(56) Grossmann, T. N.; Yeh, J. T.-H.; Bowman, B. R.; Chu, Q.; Moellering, R. E.; Verdine, G. L. Inhibition of oncogenic Wnt signaling through direct targeting of β-catenin. *Proc. Natl. Acad. Sci. U. S. A.* **2012**, *109*, 17942−19747.
(57) Huang, Z.; Zhang, M.; Burton, S. D.; Katsakhyan, L. N.; Ji, H. Targeting the Tcf4 $G^{13}ANDE^{17}$ binding site to selectivity disrupt β-catenin/T-cell factor protein−protein interactions. *ACS Chem. Biol.* **2014**, *9*, 193−201.
(58) Zhang, M.; Huang, Z.; Yu, B.; Ji, H. New homogeneous high-throughput assays for inhibitors of β-catenin/Tcf protein−protein interactions. *Anal. Biochem.* **2012**, *424*, 57−63.
(59) Mysinger, M. M.; Weiss, D. R.; Ziarek, J. J.; Gravel, S.; Doak, A. K.; Karpiak, J.; Heveker, N.; Shoichet, B. K.; Volkman, B. F. Structure-

DOI: 10.1021/acs.jmedchem.5b00223
J. Med. Chem. XXXX, XXX, XXX−XXX

based ligand discovery for the protein−protein interface of chemokine receptor CXCR4. *Proc. Natl. Acad. Sci. U. S. A.* **2012**, *109*, 5517−5522.
(60) Roubínek, F.; Bydžovský, V.; Buděšínský, Z. Substituted 5- and 6-quinoxalinecarboxylic acids and their tuberculostatic activity. *Collect. Czech. Chem. Commun.* **1984**, *49*, 285−294.
(61) Zhang, M.; Catrow, J. L.; Ji, H. High-throughput selectivity assays for small-molecule inhibitors of β-catenin/T-cell factor protein−protein interactions. *ACS Med. Chem. Lett.* **2013**, *4*, 306−311.
(62) Guedat, P.; Jacq, X.; Colland, F.; Daviet, L.; Formstecher, E.; Rain, J.-C.; Colombo, M. Preparation of tetracyclic compounds as cysteine proteases inhibitors. U.S. Patent 7,875,613, January 25, 2011.
(63) Gaillard, P.; Quattropani, A.; Pomel, V.; Rueckle, T.; Klicic, J.; Church, D. Preparation of pyrazine derivatives, particularly *N*-[3-(oxyphenylamino)quinoxalin-2-yl]sulfonamides, as PI3K inhibitors. U.S. Patent 8,071,597, December 6, 2011.
(64) Korinek, V.; Barker, N.; Morin, P. J.; van Wichen, D.; de Weger, R.; Kinzler, K. W.; Vogelstein, B.; Clevers, H. Constitutive transcriptional activation by a β-catenin−Tcf complex in $APC^{-/-}$ colon carcinoma. *Science* **1997**, *275*, 1784−1787.
(65) Ilyas, M.; Tomlinson, I. P. M.; Rowan, A.; Pignatelli, M.; Bodmer, W. F. β-Catenin mutations in cell lines established from human colorectal cancers. *Proc. Natl. Acad. Sci. U. S. A.* **1997**, *94*, 10330−10334.
(66) Sparks, A. B.; Morin, P. J.; Vogelstein, B.; Kinzler, K. W. Mutational analysis of the APC/β-catenin/Tcf pathway in colorectal cancer. *Cancer Res.* **1998**, *58*, 1130−1134.
(67) Leung, J. Y.; Kolligs, F. T.; Wu, R.; Zhai, Y.; Kuick, R.; Hanash, S.; Cho, K. R.; Fearon, E. R. Activation of *AXIN2* expression by β-catenin−T cell factor. A feedback repressor pathway regulating Wnt signaling. *J. Biol. Chem.* **2002**, *277*, 21657−21665.
(68) Jadhav, A.; Ferreira, R. S.; Klumpp, C.; Mott, B. T.; Austin, C. P.; Inglese, J.; Thomas, C. J.; Maloney, D. J.; Shoichet, B. K.; Simeonov, A. Quantitative analyses of aggregation, autofluorescence, and reactivity artifacts in a screen for inhibitors of a thiol protease. *J. Med. Chem.* **2010**, *53*, 37−51.
(69) Che, J.; King, F. J.; Zhou, B.; Zhou, Y. Chemical and biological properties of frequent screening hits. *J. Chem. Inf. Model.* **2012**, *52*, 913−926.
(70) Yu, B.; Reynisson, J. Bond stability of the "undesirable" heteroatom−heteroatom molecular moieties for high-throughput screening libraries. *Eur. J. Med. Chem.* **2011**, *46*, 5833−5837.
(71) Metz, J. T.; Huth, J. R.; Hajduk, P. J. Enhancement of chemical rules for predicting compound reactivity towards protein thiol groups. *J. Comput.-Aided Mol. Des.* **2007**, *21*, 139−144.
(72) Huth, J. R.; Song, D.; Mendoza, R. R.; Black-Schaefer, C. L.; Mack, J. C.; Dorwin, S. A.; Ladror, U. S.; Severin, J. M.; Walter, K. A.; Bartley, D. M.; Hajduk, P. J. Toxicological evaluation of thiol-reactive compounds identified using a La assay to detect reactive molecules by nuclear magnetic resonance. *Chem. Res. Toxicol.* **2007**, *20*, 1752−1759.
(73) Dahlin, J. L.; Nissink, J. W. M.; Strasser, J. M.; Francis, S.; Higgins, L.; Zhou, H.; Zhang, Z.; Walters, M. A. PAINS in the assay: chemical mechanisms of assay interference and promiscuous enzymatic inhibition observed during a sulfhydryl-scavenging HTS. *J. Med. Chem.* **2015**, *58*, 2091−2113.
(74) Takabatake, T.; Miyazawa, T.; Hasegawa, M.; Foote, C. S. Reaction of 4,7-dimethylbenzofurazan with singlet oxygen. *Tetrahedron Lett.* **2001**, *42*, 987−989.
(75) Okabe, K.; Wada, R.; Ohno, K.-i.; Uchiyama, S.; Santa, T.; Imai, K. Development of hydrophilic fluorogenic derivatization reagents for thiols: 4-(*N*-acetylaminosulfonyl)-7-fluoro-2,1,3-benzoxadiazole and 4-(*N*-trichloroacetylaminosulfonyl)-7-fluoro-2,1,3-benzoxadiazole. *J. Chromatogr., A* **2002**, *982*, 111−118.
(76) Řeha, D.; Kabeláč, M.; Ryjáček, F.; Šponer, J.; Šponer, J. E.; Elstner, M.; Suhai, S.; Hobza, P. Intercalators. 1. Nature of stacking interactions between intercalators (ethidium, daunomycin, ellipticine, and 4′,6-diaminide-2-phenylindole) and DNA base pairs. Ab initio quantum chemical, density functional theory, and empirical potential study. *J. Am. Chem. Soc.* **2002**, *124*, 3366−3376.
(77) Reynisson, J.; Schuster, G. B.; Howerton, S. B.; Williams, L. D.; Barnett, R. N.; Cleveland, C. L.; Landman, U.; Harrit, N.; Chaires, J. B. Intercalation of trioxatriangulenium ion in DNA: binding, electron transfer, X-ray crystallography, and electronic structure. *J. Am. Chem. Soc.* **2003**, *125*, 2072−2083.
(78) Ichikawa, T.; Kato, T.; Takenishi, T. New synthesis of adenine and 4-aminoimidazole-5-carboxamide. *J. Heterocycl. Chem.* **1965**, *2*, 253−255.
(79) Trott, O.; Olson, A. J. AutoDock Vina: improving the speed and accuracy of docking with a new scoring function, efficient optimization, and multithreading. *J. Comput. Chem.* **2010**, *31*, 455−461.
(80) Friesner, R. A.; Banks, J. L.; Murphy, R. B.; Halgren, T. A.; Klicic, J. J.; Mainz, D. T.; Repasky, M. P.; Knoll, E. H.; Shelley, M.; Perry, J. K.; Shaw, D. E.; Francis, P.; Shenkin, P. S. Glide: a new approach for rapid, accurate docking and scoring. 1. Method and assessment of docking accuracy. *J. Med. Chem.* **2004**, *47*, 1739−1749.
(81) Morris, G. M.; Huey, R.; Lindstrom, W.; Sanner, M. F.; Belew, R. K.; Goodsell, D. S.; Olson, A. J. AutoDock4 and AutoDockTools4: Automated docking with selective receptor flexibility. *J. Comput. Chem.* **2009**, *30*, 2785−2791.
(82) Helissey, P.; Desbène-Finck, S.; Giorgi-Renault, S. Alkylation of 5- and 6-methylindolo[2,3-*b*]quinoxalines: revised structures of the *N*,*N*′-dimethylated salts. *Eur. J. Org. Chem.* **2005**, 410−415.
(83) Thomas, K. R. J.; Tyagi, P. Synthesis, spectra, and theoretical investigations of the triarylamines based on 6*H*-indolo[2,3-*b*]-quinoxaline. *J. Org. Chem.* **2010**, *75*, 8100−8111.
(84) Ramström, O.; Lehn, J.-M. Drug discovery by dynamic combinatorial libraries. *Nature Rev. Drug. Discovery* **2002**, *1*, 26−36.
(85) Smith, M. C.; Gestwicki, J. E. Features of protein−protein interactions that translate into potent inhibitors: topology, surface area and affinity. *Expert Rev. Mol. Med.* **2012**, *14*, e16.
(86) Nikolovska-Coleska, Z.; Wang, R.; Fang, X.; Pan, H.; Tomita, Y.; Li, P.; Roller, P. P.; Krajewski, K.; Saito, N. G.; Stuckey, J. A.; Wang, S. Development and optimization of a binding assay for the XIAP BIR3 domain using fluorescence polarization. *Anal. Biochem.* **2004**, *332*, 261−273.

DOI: 10.1021/acs.jmedchem.5b00223
J. Med. Chem. XXXX, XXX, XXX−XXX